THE ELECTRONIC ORIGIN OF PROMOTER MODES OF PROTON TRANSFER REACTIONS IN HYDROGEN BONDED SYSTEMS

Thesis Submitted for the Degree

of

DOCTOR OF PHILOSOPHY

By

BANDA SARITHA

SCHOOL OF CHEMISTRY

UNIVERSITY OF HYDERABAD

HYDERABAD 500 046

INDIA

December 2010

STATEMENT

I hereby declare that the matter embodied in this thesis is the result of investigations carried out by me in the School of Chemistry, University of Hyderabad, Hyderabad, under the supervision of Prof. M. Durga Prasad.

In keeping with the general practice of reporting scientific observations, due acknowledgement has been made wherever the work described is based on the findings of other investigators.

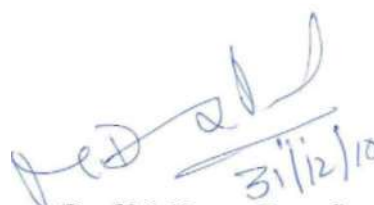Hyderabad-46   **(Banda Saritha)**

December 2010

CERTIFICATE

Certified that the work contained in this thesis entitled "The **Electronic Origin of** Promoter Modes **of Proton Transfer Reactions in Hydrogen Bonded** Systems" has been carried out by Ms. BANDA SARITHA under my supervision and the same has not been submitted elsewhere for a degree.

Hyderabad-46

December 2010

(Prof M. Durga Prasad)

Thesis Supervisor

School of Chemistry,
University of Hyderabad,
Hyderabad-500 046, India

Dean

School of Chemistry

University of Hyderabad

Hyderabad 500 046

INDIA   Dean
School of Chemistry
University of Hyderabad
Hyderabad - 500 046

n

ACKNOWLEDGMENT

It is my privileged opportunity to acknowledge and give thanks to all who have contributed to my Ph. D and my life in the University of Hyderabad. First, I would like to express my immense gratitude and sincere thanks to my supervisor. **Prof. M. Durga Prasad** for his corrections, rebuke, and teaching and guiding me throughout my research work. Your kindness and command over the subject will always inspire me.

It has been a great and exciting experience to study at the School of Chemistry. My sincere thanks to the former and present Deans and all faculty members for their support during my Masters and Ph.D.

I want to thank Prof. T. P. Radha Krishan for the M. Sc project and Dr. S. K. Das for giving me an opportunity to work in his lab for one year.

I am very thankful for Advanced Center for Research in High Energy Materials ACRHEM), University of Hyderabad, for the financial support for the first two years of my Ph.D and DST/IBM for the subsequent three years. Centre for Modelling Simulation and Design (CMSD), University of Hyderabad, for computational facilities.

I want to thank all the non-teaching staff for their help and co-operation.

'. am thankful to my lab mates Tapta Kanchan Roy. V.V.G.P Kumar, Sreedhar Reddy, Dinesh for their help and co-operation and making lab a pleasant place to work. I am thankful to Shiva, Tanmoy Mondal, Susanta Ganta Rajagopal,

Dedicated to

Lord Jesus Christ – the way, the truth and the life

and

All the teachers who taught me the value of learning

CONTENTS

CHAPTER 1

INTRODUCTION

1.1. PRELIMINARY REMARKS

Hydrogen transfer is a common step in several molecular processes of chemical and biological intrest[1-7]. Several studies have been carried out to understand the dynamics of such process over the past several years. Potential energy surfaces have been calculated for several systems and vibrational energy level calculations have been carried out to determine the tunneling splittings[8-13]. Several efforts have been directed towards calculation of rate constants for such reactions[14]. These include variational transition state theory based approaches[15-17], semi-classical instanton methods[18-23] and direct dynamics[24] on the relevant regions of the potential energy surfaces. Single and concerted multiple proton transfers that go through a single transition state have been considered both theoretically[25, 26] and experimentally[27-33].

Within the frame work of Born-Oppenheimer approximation, the dynamics of a reaction is controlled by the underlying potential energy surface. The potential energy surfaces (PES) of intermolecular proton transfer in hydrogen bonded donor-acceptor complexes fall into a special class. Both the minima, representing the reactant and product structures, are quiet close to each other in the configuration space of these systems. However, they are separated by a large barrier along the path that connects the two structures directly. Computationally, it is observed that the transition state (TS) is displaced along a direction orthogonal to this direct path in practically all the systems that have been studied so far [8-26]. The consequent drop in the threshold energy for crossing the barrier is quite significant. As a result, the intrinsic reaction co-ordinate (IRC) that connects the reactant and product through the transition state is essentially the direction of this orthogonal mode near the reactant and product structures, and becomes the proton motion only in the vicinity of the transition state. Increased vibration motion along this orthogonal direction enhances the overall rate of the reaction significantly[34]. Such modes have been termed the promoter modes in the literature.

Several efforts were made to identify and characterize the promoting vibrations. It was noted that if a mode is symmetrically coupled to the proton transfer co-ordinate, the rate of the proton transfer reaction increases relative to the reaction without such symmetric coupling. The reason for this is that the

effective barrier to the proton transfer decreases as a system moves along the symmetrically coupled mode in one direction[34-36.]

To understand the nature and effect of promoter modes, model potentials that mimic these effects were constructed. The proton transfer co-ordinate is modeled often by a symmetric double well potential represented as a quatric potential[34]

$$V_p(q) = V_0 (q^2 - 1)^2 \qquad (1.1)$$

Here, V_0 is the barrier height and the two minima are at $q = \pm 1$. The promoting mode is taken to be governed by a harmonic potential and symmetrically coupled to the proton transfer co-ordinate. So, the full potential for these two dimensional system is represented as

$$V(q, Q_s) = V_p(q) + \frac{1}{2} \omega_s^2 (Q_s + \frac{c_s q^2}{\omega_s^2})^2 \qquad (1.2)$$

This model predicts the increase of the barrier frequency at the transition state correctly. However, it does not predict the reduction in the barrier height as one move along the symmetric mode. One feature of this model is that the system moves along the symmetrically coupled co-ordinate upto a point, before the proton transfer occurs. After the proton jumps to its destination the system retreats along the symmetrically coupled co-ordinate. This mimics the nature of the promoting mode correctly.

An alternative group of modes have also been considered by earlier authors[34-37]. The potential and coupling of these modes is posited to be

$$V_a = \frac{1}{2}\omega_a^2(q_a - \frac{c_a q}{\omega_a^2})^2 \qquad (1.3)$$

Unlike the symmetric mode (which does not undergo a net displacement during the proton transfer reaction) this antisymmetric mode does undergo a net displacement during the course of the reaction. Cui and Karplus[34] named it as the demoter mode. The reasons for this nomenclature are two. First, because the system undergoes a net displacement along the antisymmetric co-ordinates, there is a Frank-Condon factor in the over all rate expression in the sense of Marcus theory of electron transfer reactions. Second, the effective barrier frequency at the transition state decreases in these systems due to the antisymmetric bilinear coupling. As a result, the tunneling becomes less favorable, reducing the overall rate constant. Cui and Karplus have made an extensive study of the influence of the both the types of modes on the overall rate of a reaction. These conclusions may be summarized as follows.

Motion along the direction of symmetrically coupled mode enhances the rate constant compared to the uncoupled reaction. This effect depends on the system under consideration and the temperature. In the high temperature limit the increase in the rate constant is primarily due to the lowering of the effective barrier along the proton transfer co-ordinate. As a result of the reduced barrier, the effective, over-the-barrier reactive flux increases exponentially since the barrier appears in an exponential function. In this sense the effect of the

symmetrically coupled co-ordinates is primarily on the classical part of the rate constant. In fact, the contribution of tunneling to the overall rate decreases. In the low temperature limit, on the other hand, the rate increases because the contribution of tunneling increases. This is due to the reduction in the barrier frequency. We recall in this context that the tunneling factor is given by

$$\kappa = \frac{\beta\hbar\omega/2}{\sin(\frac{\beta\hbar\omega}{2})}, \qquad (1.4)$$

in the semi classical limit. As can be seen the tunneling factor at low temperatures increases with increasing ω value.

The antisymmetrically coupled modes on the other hand tend to reduce the rate constant relative to the uncoupled rate constant. For one, such a coupling lowers the effective barrier frequency and this in turn leads to a reduction of the tunneling probability. Second, the antisymmetric coupling gives rise to an asymmetry in the effective potential along the proton transfer co-ordinate. This also reduces tunneling except in the vicinity of the transition state. The effective potential to the proton transfer becomes more symmetric if the antisymmetrically mode is excited. Under these conditions the tunneling rate would increase. As we noted earlier, the antisymmetrically coupled modes undergo a net displacement during the course of the reaction. In that sense, these should be treated as a part of the overall reaction co-ordinate. However, as we shall see in the examples to be discussed latter, the major changes along these co-ordinates are not synchronous with the proton transfer co-ordinate. A schematic picture of the behavior of these two co-ordinates and the proton transfer co-ordinate is given

by Cui and Karplus (Fig. 2b of Ref. 34 for the symmetrically coupled co-ordinate and Fig. 3b for the antisymmetrically coupled co-ordinate).

In the next section we summarize the calculations on the potential energy surfaces to identify the symmetric and antisymmetrically coupled co-ordinates in these systems.

1.2. A BRIEF REVIEW OF *ABINITIO* POTENTIAL ENERGY SURFACE FOR SOME PROTON TRANSFER REACTIONS.

In this section we describe the potential energy surfaces for some of the systems that have been reported in the literature. We analyze the surfaces to identify the promoting and demoting vibrations in those systems. Most of the systems are fairly large and are not amenable for the development of the full potential energy surface. Consequently, most of the authors have constructed reduced dimensional PES. The systems that have received particular attention are formic acid dimer (FAD), hydrogen fluoride clusters, malonaldehyde (MA), tropolone (TrOH) and several water clusters. We discuss the PES of these systems below.

1.2.1 PES OF FAD

The first attempt to describe the PES of FAD is by Shida *et al*[9b, 37]. In their first effort[9b] they constructed an adiabatic reaction surface. Shida *et al* used six internal co-ordinates as independent variables. Using symmetry arguments they

reduced the number to three independent variables. The first of these is the symmetrized movement of the protons, the second is the average distance between the donor and acceptor and the third is the antisymmetric proton movement. Various cuts of the potential were presented. From Fig. 2 of their work, it is apparent that the second mode (donor-acceptor distance) is symmetrically coupled to the first mode (proton transfer co-ordinate). Obviously the donor acceptor distance plays the role of a promoter mode according to the Cui–Karplus criteria. Later they have analyzed various possible paths for the system on the PES they have constructed[37]. These are the usual minimum energy path (MEP), the maximum probability path (MPP) based on the vibrational ground state wave function, an approximated MPP termed the normal vibration path (NVP), a straight line path between reactant and product (SLP) and the expectation value path (EVP). One curious observation of their studies is that the MPP is half way between the MEP and SLP. Not withstanding this, the three representations of the reaction path (MEP, NVP and MPP) indicate that, the first part of the reaction path is dominated by the changes in the donor-acceptor distance and the central region (around the TS) is dominated by the proton transfer co-ordinate (Fig. 10 and 11 of Ref . 9b).

Lorting and Liedl analyzed[17c] the PES of FAD interms of the normal modes of the system. They concluded that four modes are significant in this reaction. These are the symmetric H transfer, interdimer stretch, CO_2 rocking and CO_2 bending. From the data they have presented (Fig. 3 of Ref. 17c). The

interdimer stretch and CO_2 bending play the role of promoter modes because they undergo no net displacement at the end of the reaction. On the other hand the CO_2 rocking shows a clear net displacement and hence should be interpreted as a demoter mode. Intrestingly this mode undergoes half of its net displacement before IRC = –0.5 and the other half after IRC ≥ 0.5. In the intermediate region, the symmetric hydrogen stretch goes through most of its change (about 0.6 against about 0.4 in the rest of the IRC).

Sibert and co-workers carried out an extensive analysis of the FAD system[9a, 10, 11a, 38]. They have used the normal modes of the system at the transition state as the basis. They found that the three co-ordinates are essential for the construction of a reaction surface Hamiltonian. These are the symmetric OH stretch, the symmetric dimer rock and the dimer stretch. The symmetric OH stretch is obviously the proton transfer co-ordinate. They have provided the cuts of the PES along the OH stretch and the dimer stretch, and the OH stretch and the dimer rock respectively (Fig. 1 of Ref. 9a). From this figure it is clear that the dimer stretch is symmetrically coupled to the proton transfer co-ordinate and suffers no net displacement at the end of the reaction. On the other hand, the dimer rock is antisymmetrically coupled to the proton transfer co-ordinate and undergoes a net displacement during the course of the reaction. From this it is obvious the dimer stretch plays the role of a promoter mode, while the dimer rock plays the role of a demoter mode according to the Cui–Karplus definitions. Note that these two modes are also the ones identified by Loerting and Liedl. The CO_2

bend mode undergoes very little displacement during the course of the proton transfer. Presumably for this reaction Sibert and co-workers had not considered it in their study.

Fig. 1.1: The structure of FAD at a) Reactant and b) The Transition state. The structural parameters are presented in Appendix A.
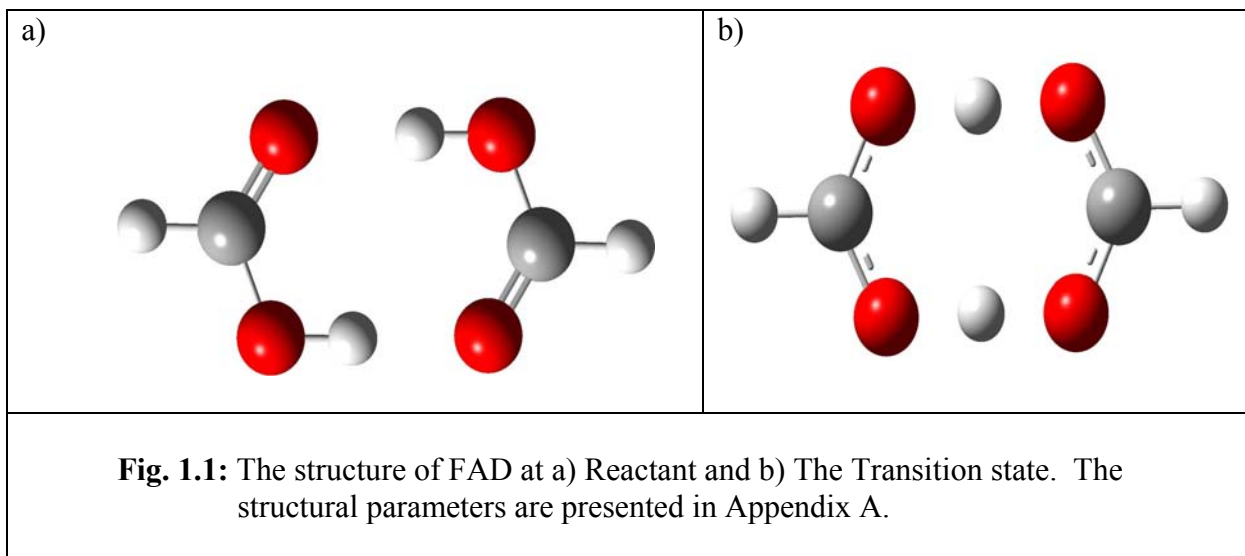
In addition to these studies on the PES, these authors and others[8a] have also calculated the vibrational wave functions and tunneling splittings in these levels for FAD.

1.2.2 PES Of (HF)$_n$-Clusters

Liedl and co-workers[17e] made an extensive study of proton transfer reactions in cyclic HF clusters at different levels of theory. These molecules have C_{nh} symmetry in the equilibrium structure and undergo a synchronous n proton transfer through a D_{nh} transition state. They concluded[17e] that three modes are sufficient to represent the symmetric transition from C_{nh} equilibrium to other C_{nh} equilibrium structure through the D_{nh} transition state. These modes are the symmetric HF, the symmetric FF stretch modes and the symmetric bending vibrations[17e]. From the cut of the PES in the first two modes for (HF)$_5$ systems (Fig. 4 of Ref. 17e). It is apparent that the symmetric FF stretch is symmetrically coupled to the proton transfer co-ordinate[17e] and thus plays the role of a promoter mode. They have also noted that the symmetric bending mode undergoes very little displacement along the IRC, and thus is expected to be coupled to the reaction co-ordinate rather weakly. They analyzed the displacements of different normal modes along the IRC in Ref. 15. From Fig. 5 of this reference it is seen that the movement along the proton transfer co-ordinate is sluggish in the initial part of the IRC (IRC <–0.5) and remains constant in the next 1 unit of IRC. The bend mode also shows similar behavior though not as sharp as in the FF stretch mode. From the foregoing it is obvious that the FF stretch mode and the symmetric hydrogen bend mode play the role of promoter modes for this class of systems. No demoter modes appear to be present here.

Fig. 1.2: The structure of $(HF)_3$ at a) Reactant and b) The Transition state. The structural parameters are presented in Appendix A.
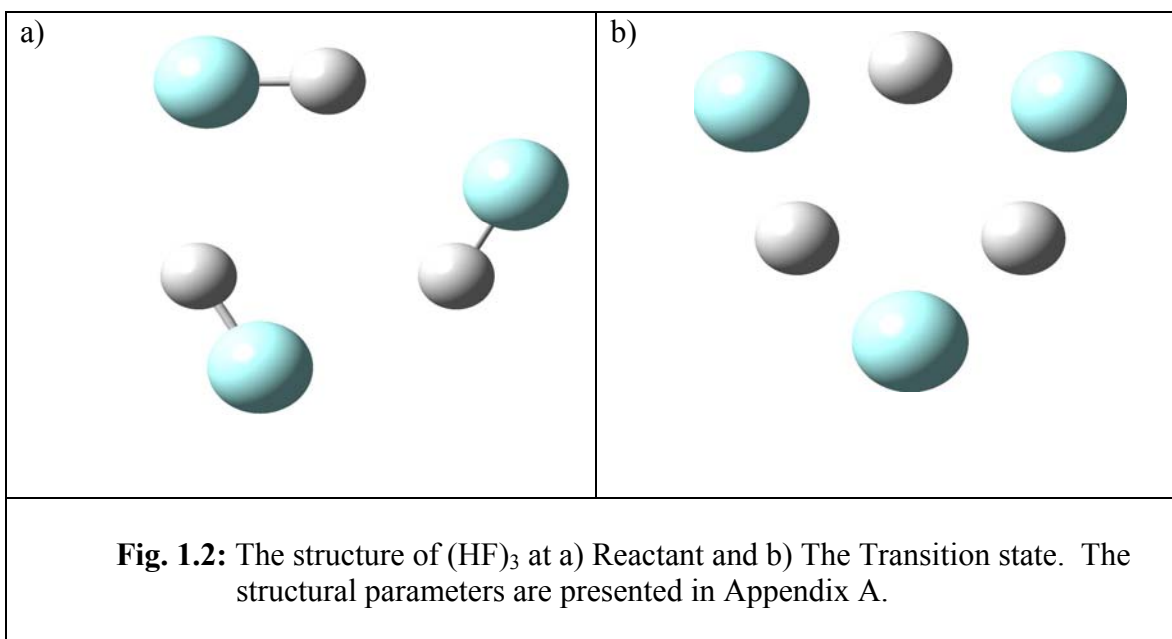
1.2.3 PES OF MALONALDEHYDE

The PES for the proton transfer in malonaldehyde was first reported by Carrington and Miller[39]. They have used the two OH distances (r_1, r_2) to construct a reduced two dimensional reaction surface Hamiltonian. The potential surface was evaluated at the minimum basis (SCF) level of theory. From the presented potential energy surface (Fig. 1 of Ref. 39). It is obvious that $r_1 - r_2$ is the proton transfer co-ordinate and $r_1 + r_2$ is a measure of the distance between the donor and acceptor oxygen atoms. Here r_1 and r_2 are the distances of the hydrogen from the two oxygen atoms. Using this PES they have calculated the tunneling splittings in

malonaldehyde. In a later effort Makri and Miller[40] calculated the tunneling splittings in malonaldehyde using a new semi classical tunneling model.

Fig. 1.3: The structure of malonaldehyde at a) Reactant and b) The Transition state. The structural parameters are presented in Appendix A.
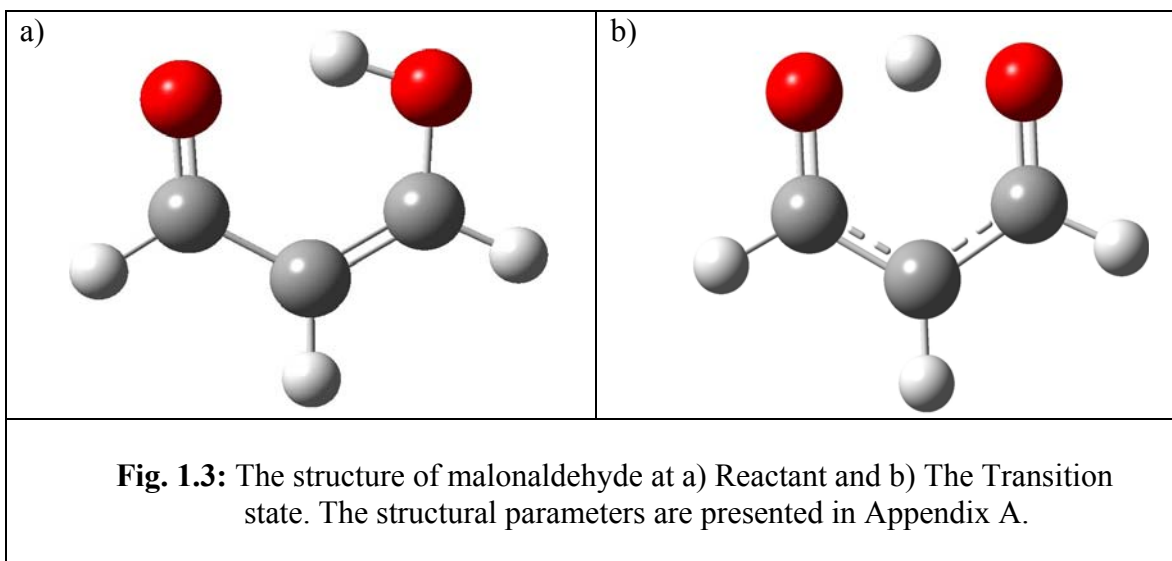
Shida *et al*[41] have investigated various aspects of intramolecular proton transfer reaction in malonaldehyde within the framework of reaction surface Hamiltonian. They noted that the heavy atom motion (stretching motion between two oxygen atoms) is the main character of IRC as the molecule moves from the equilibrium geometry towards the saddle point. Near the saddle point the IRC is primarily hydrogenic motion. The IRC is sharply curved as a consequence, and the actual dynamic motion is expected to deviate from the IRC. They have developed a reaction surface of three co-ordinates r_1 and r_2 of Carrington and Milller and the displacement of O---O distance r_3. The electronic structure calculation had a combination of *ab initio* SCF and *ab initio* modified coupled pair calculations to

incorporate the dynamic correlation effects in a size consistent manner. The vibrational wave functions on these surfaces were determined and various tunneling paths were identified. Two new mass weighted co-ordinates $q_1 \approx r_1 - r_2$ and $q_2 \approx r_1 + r_2$ were defined to understand the nature of the reaction path. A cut of the PES in the space of q_1 and q_2 shows clearly that the q_1 is the proton transfer co-ordinate and q_2 is a promoter mode. It is coupled symmetrically to q_1 and goes through zero net displacement during the course of the reaction. They have analyzed interplay of potential energy and mass. The minimum energy path has a significantly smaller barrier than the expectation value path. On the other hand the expectation value barrier is narrower. Since the effective mass along this path is large. From this they concluded that the tunneling is more effective along EVP notwithstanding the large barrier along this path. Yagi *et al*[42] have generated the full dimensional PES for the hydrogen atom transfer reaction in malonaldehyde. They have used a modified Sheppard interpolation method with a MP2 level of calculation for the individual points. The reference points have been set along the reaction path of the hydrogen atom. Cuts of the potential energy surface in a two dimensional subspace spanned by the vector defining the difference between the reactant and product and the vector representing the displacement of the transition state from the reactant is presented (Fig. 4 of Ref. 42). The presented surface clearly shows the curved nature of the IRC and the promoting nature of the second vector.

More recently Tew et al^{43} have constructed a reduced two dimensional reaction surface Hamiltonian for malonaldehyde. They have opted to define the reaction surface Hamiltonian in terms of two co-ordinates r_1 and r_2 defined by Carrigton and Miller earlier[39]. They have symmetrized the two co-ordinates by defining $q_1 = (r_1+r_2)/2$ and $q_2 = (r_1-r_2)/2$. The antisymmetric combination looks like proton transfer co-ordinate, and q_1 looks like the displacement vector between donor and acceptor. The reaction surface is evaluated by constrained geometry optimizations on a grid of q_1 and q_2. The electronic barrier at each grid point was determined on MP2/6-31g** calculation. The plot of the reaction surface (Fig. 2 of Ref. 43) shows clearly that q_1 is the reaction co-ordinate at the transition state and q_2 which dominates the IRC in the initial and final parts of reaction path is the promoter mode.

In addition to these studies several other studies have been made on this system. Thus, Liedl and co-workers[44] analyzed the nature of the optimal tunneling path for the proton transfer. Manthe and co-workers[45] have calculated the tunneling splitting using MCTDH approach and the diffusion Monte Carlo based projection operator, imaginary time spectral time evolution methods. Bowman co-workers[46] have calculated the ground state tunneling splitting using diffusion Monte Carlo method in Cartesian and transition state normal co-ordinates.

1.2.4 PES OF TROPOLONE

The first calculation on the PES of tropolone is by Verner and co-workers[47]. They have used three co-ordinates for describing the reduced dimensional PES. These are the OH bond length(r) the O---O distance (R) and the angle between them (θ). *Ab initio* method at SCF level with 6-31g basis were used to generate the electronic energy over the grid. The other degree of freedom were optimized for a given set of values of r, R and θ to provide the adiabatic PES. They have also presented the PES on the S_1 Surface (Fig. 2 of Ref. 47). Two of the important conclusions they have reached are (1) the O---O vibrations are strongly coupled to the proton transfer co-ordinate causing proton transfer stretching vibrational level splitting and (2) the deformation vibrations coupled to the proton transfer motion rather weakly. This study indicates the O---O stretching behaves like a promoter mode for the proton transfer in this system. They have also noted that the O---O stretching frequency remains more are less constant. More recently Giese and Kühn have constructed an all Cartesian reaction plane Hamiltonian for Tropolone[48]. They have provided a cut of the PES along two co-ordinates d_1 and d_2. Here, d_1 is the unit vector from reactant configuration to product configuration and d_2 is the unit vector from the mid point between reactant and product configuration towards the transition state configuration. Fig. 3 of Ref. 48 clearly shows that the IRC is essentially d_1 in the vicinity of the transition state. Note that this is predominantly the proton transfer co-ordinate though it also consists of the co-ordinates representing the π bond reorganization.

Fig. 1.4: The structure of tropolone at a) The Reactant and b) The Transition state.
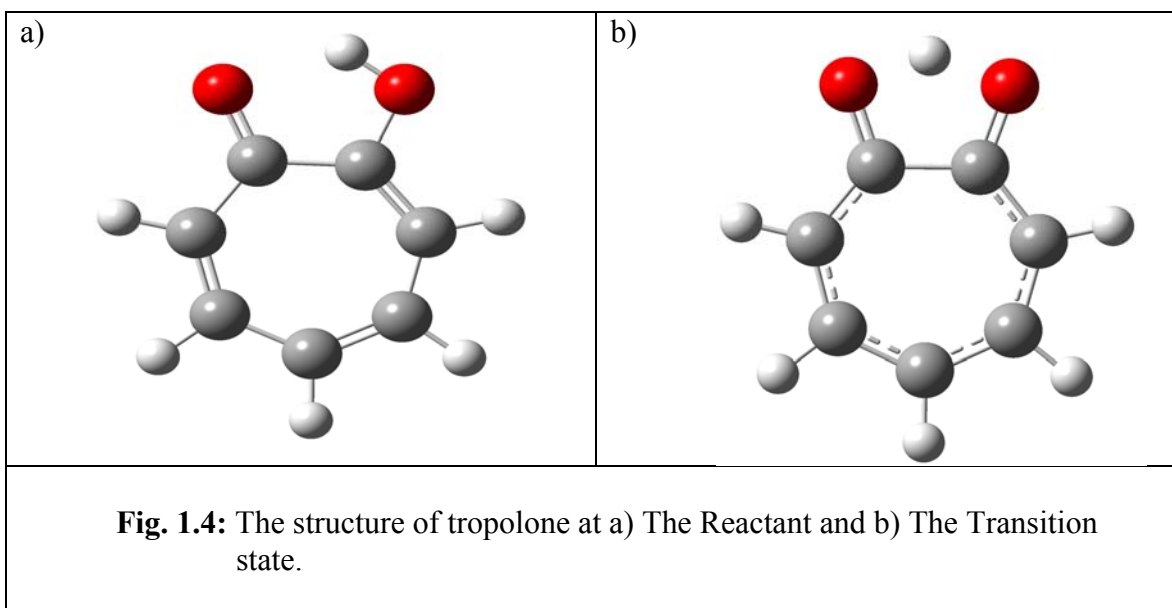
The rest of the IRC is essentially d_2 like which consists of essentially the O---O displacement vector. They have analyzed the intrinsic reaction path and variation of vibrational frequencies along it. They have also calculated some of the vibrational states on this potential energy surface.

1.2.5 OTHER SYSTEMS

Gil and Waluk[49] have noted that the hydrogen tunneling in porphecene proceeds as a thermally activated double hydrogen tunneling. The barrier to the reaction is modulated by a vibration that simultaneously changes the strength of the two hydrogen bonds. Their conclusion is based on an analysis of the experimental

fluroscence anisotropy data rather than from *ab initio* calculation of the relevant PES.

Sarai[50] constructed a PES for tetra phenyl porphin using by CNDO method. He has used two co-ordinates r_1 and r_2, the distances of the protons measured from the center of the adjacent nitrogen atoms. He concluded that the proton migration process is strongly coupled to the symmetry breaking deformation of the porphin skeleton.

1.2.6 SUMMARY

As we noted in introduction the two minima corresponding to the reactant and product structure are quite close to each other in configuration space in proton transfer reactions separated by a large barrier along the straight line path between these two structures. As the discussion above shows, the barrier drops significantly when the system moves along an orthogonal path to the straight line path. This orthogonal path primarily consists of heavy atom motion in which the donor and acceptor atoms come closer. It can not be represented by a single normal mode at the saddle point. For example in the FAD the interdimer stretch and the symmetric OCO bending modes contribute to this motion. Similarly in the cyclic HF clusters the symmetric FF stretch and the inplane symmetric HF bend contribute to such a promoting mode. In addition to these there are demoting modes in some cases. For example the OCO antisymmetric stretch in FAD is one such. Indeed, in all systems involving π bonds, there would be a

reorganization of the π network. Modes involved in such reorganization would have to be classified as demoter modes. Curiously, in all the surfaces that have been reported to date, the motion along the promoter seems to be both before and after the proton migration but rarely concurrent with it.

1.3 GOALS OF THE PRESENT WORK

Our goal in this work is to explore the electronic origin of the promoter modes. The specific question we ask is, "what are the changes in the electronic structure that cause a reduction in the barrier height to the proton transfer as the molecular system moves along the promoter mode?". In a proton exchanging hydrogen bonded complex, the acceptor atom has a lone pair oriented towards the hydrogen atom bound to the donor moiety. We suggest that, as the complex moves along the promoter mode, the acceptor atom donates its lone pair into the antibonding orbital of the sigma bond between the hydrogen and donor atom. As a consequence, the bond between these two atoms is weakened to a significantly greater extent than at the reactant equilibrium geometry, and the proton transfer goes through a smaller barrier. We provide computational evidence supporting this proposition using natural bond orbital (NBO) analysis. The computational methodologies used for this study are summarized in Chapter 2. Studies on two systems, formic acid dimer (FAD) and cyclic HF-trimer, are presented in Section 3. Several physically relevant quantities, such as the vibrational frequencies are affected by such donations. Some of these are also explored in chapter 3.

In systems in which the donor and acceptor atoms are distinct, and, are part of a π-network, the π bonds reorganize themselves to compensate the charge imbalance due to the proton transfer. The sequence in which such changes occur with reference to the proton transfer is the subject of chapter 4. We look at the π reorganization in two systems, FAD and MA here.

Next we look at the implications of the charge donation from the acceptor to the antibonding orbital of D-H bond for kinetic isotope effect in Chapter 5. It turns out that because of the charge donation, not only does the frequency of the proton transfer coordinate turn imaginary at the saddle point, but, in multi proton transfer systems, all other proton stretch frequencies fall significantly(by about 50%) at the TS. This fall is almost linearly dependent on the number of protons that are undergoing a synchronous transfer. We confirm this by studying three classes of systems, FAD, $(HF)_3$ and $(H_2O)_n$ ($3 \leq n \leq 6$). Since the decrease in the zero point energy is linearly proportional to the number of protons transferred, the kinetic isotope effect (k_H/k_D) increases exponentially.

Finally, we summarize our findings in Chapter 6.

REFERENCES

(1) Spies, M. A.; Toney, M. D. *Hydrogen Transfer Reactions;* Wiley: New
York, **2007** *, 3,* 1139.

(2) Smedarchina, Z.; Siebrand, W.; Fernández-Ramos, A.; Cui, Q. *J. Am. Chem.
Soc.* **2003**, *125*, 243.

(3) Gora, R. W.; Grabowski, S. J.; Leszczynski, J. *J. Phys. Chem. A* **2005***, 109,*
6397.

(4) Gilli, P.; Bertolasi, V.; Ferretti, V.; Gilli, G. *J. Am. Chem. Soc.* **1994***, 116,*
909.

(5) Bertran, J.; Oliva, A.; Rodríguez-Santiago, L.; Sodupe, M. *J. Am. Chem. Soc.*
1998, *120,* 8159.

(6) (a) Scheiner, S.; Kern, C. W. *J. Am. Chem. Soc.* **1979**, *101,* 4081. (b) Bene,
J. E. D. *J. Chem. Phys.* **1975***, 62*, 1314.

(7) Borgis, D.; Hynes, J. T. *Chem. Phys.* **1993**, *170*, 315.

(8) (a) Luckhaus, D. *J. Phys. Chem. A* **2006***, 110,* 3151. (b) Wang, Y.; Braams, B.
J.; Bowman, J. M.; Carter, S.; Tew, D. P. *J. Chem. Phys.* **2008**, *128*, 224314.
(c) Vener, M. V.; Kühn, O.; Bowman, J. M. *Chem. Phys. Lett.* **2001**, *349*,
562.

(9) (a) Barnes, G. L.; Squires, S. M.; Sibert III, E. L. *J. Phys. Chem.* B **2008***,
112,* 595. (b) Shida, N.; Barbara, P. F.; Almlöf, J. *J. Chem. Phys.* **1991**, *94*,
3633.

(10) Barnes, G. L.; Sibert III, E. L. *J. Mol. Spectr.* **2008**, *249***,** 78.

(11) Barnes, G. L.; Sibert III, E. L. *Chem. Phys. Lett.* **2008,** *460***,** 42.

(12)(a) Matanović, I.; Došlić, N. Kühn, O. *J. Chem. Phys.* **2007***, 127,* 014309.

(b) Matanović, I.; Došlić, N.; Johnson, B. R. *J. Chem. Phys.* **2008**, *128*, 084103.

(13) Tautermann, C. S.;Voegele, A. F.; Liedl, K. R. *J. Chem. Phys.* **2004,** *120,* 631.

(14) Matanović, I.; Došlić, N. *Chem. Phys.* **2007**, *338,* 121.

(15) Loerting, T.; Liedl, K. R. *J. Phys. Chem. A* **1999***, 103,* 9022.

(16) Loerting. T.; Liedl, K. R.; Rode, B. M. *J. Chem. Phys.* **1998***, 109,* 2672.

(17) (a) Tautermann, C. S.; Loferer, M. J.; Voegele, A. F.; Liedl. K. R. *J. Chem. Phys.* **2004**, *120*, 11650. (b) Loerting, T.; Liedl, K. R.; Rode, B. M. *J. Am. Chem. Soc.* **1998**, *120*, 404. (c) Loerting, T.; Liedl, K. R. *J. Am. Chem. Soc.* **1998**, *120*, 12595. (d) Liedl, K. R.; Sekušak, S.; Kroemer, R.T.; Rode, B. M. *J. Phys. Chem. A* **1997**, *101*, 4707. (e) Liedl, K. R.; Kromer, R. T.; Rode, B. M. *Chem. Phys. Lett.* **1995**, *246*, 455.

(18) Smedarchina, Z.; Siebrand, W.; Zgierski. M. Z. *J. Chem. Phys.* **1996,** *104*, 1203.

(19) (a) Smedarchina.Z.; Siebrand. W.; Fernández-Ramos. A. *J. Chem. Phys.* **2007**, *127*, 174513. (b) Smedarchina, Z.; Fernández-Ramos, A.; Siebrand, W. *Chem. Phys. Lett.* **2004**, *395*, 339.

(20) Smedarchina, Z.; Fernández-Ramos, A.; Siebrand, W. *J. Chem. Phys.* **2005**, *122*, 134309.

(21) Smedarchina, Z.; Siebrand, W.; Zgierski. M. Z. *J. Chem. Phys.* **1995**, *103*, 5326.

(22) Smedarchina, Z.; Zgierski, M. Z.; Siebrand, W.; Kozlowski, P. M.
J. Chem. Phys. **1998**, *109***,** 1014.

(23) Benderskii,V.A.; Makarov, D. E.; Charles. A. W.; *Advan. Chem. Phys*;
Wiley: New York, LXXXVIII, **1994**.

(24) (a) Kim**,** Y. *J. Am. Chem. Soc.* **1996,** *118*, 1522. (b) Markwick, P. R.;
Doltsinis, N. L.; Marx, D. *J. Chem. Phys.* **2005**, *122*, 054112.

(25) Tautermann, C. S.; Voegele, A. F.; Loerting, T.; Liedl, K. R. *J. Chem. Phys.*
2002, *117*, 1962.

(26) Tautermann, C. S.; Voegele, A. F.; Loerting, T. *J. Chem. Phys.* **2002**, *117*,
1967.

(27) Schlabach, M.; Limbach, H-H.; Bunnenberg, E.; Shu, A. Y. L.; Tolf, B. R.;
Djerassi, C. *J. Am. Chem. Soc*. **1993**, *115*, 4554.

(28) (a) Scherer, G.; Limbach, H-H. *J. Am. Chem. Soc*. **1994**, *116*, 1230. (b)
Scherer, G.; Limbach, H-H. *J. Am. Chem. Soc*. **1989**, *111*, 5946. (c)
Meschede, L; Limbach, H-H. *J. Phys. Chem.* **1991,** *95*, 10267. (d) Gerritzen,
D.; Limbach, H-H. *J. Am. Chem. Soc.* **1984**, *106*, 869.

(29) Ortlieb, M.; Havenith, M. *J. Phys. Chem. A* **2007**, *111*, 7355.

(30) (a) Ito, F. *J. Chem. Phys.* **2008***, 128,* 114310*.* (b) Ito, F. Nakanaga, T. *Chem. Phys.* **2002***, 227,* 163.

(31) Florio, G. M.; Zwier, T.S.; Myshakin, E. M.; Jordan, K. D.; Sibert III, E. L.
J. Chem. Phys. **2003***, 118,* 1735.

(32) Meyer, R.; Ernst, R. R. *J. Chem. Phys.* **1990**, *93*, 5518.

(33) Stöckli, A.; Meier, B. H.; Kreis, R.; Meyer, R.; Ernst, R. R. *J. Chem. Phys.*

1990, *93*, 1502.

(34) Cui, Q.; Karplus, M. *J. Phys. Chem. B* **2002**, *106*, 7927.

(35) (a)Caratzoulas, S.; Schwartz, S. D. *J. Chem. Phys.* **2001**, *114*, 2910. (b)
Zwan, G. V, Hynes, J. T. Hynes, *Chem. Phys.* **1984**, *90* ,21. (c) Antoniou, D.;
Schwartz, S. D. *J. Chem. Phys.* **1998**, *108*, 3620 (d) Antoniou, D.; Schwartz,
S. D. *J. Chem. Phys.* **1998**, *109*, 2287.

(36) (a)Rudd, P. M.; Biochemistry **1994**, *33*, 17. (b) Benderskii, V.; Goldanskii,
V.; Makarov, D.; *Chem. Phys. Lett.* 1990, *171*, 91. (c) Benderskii, V.;
Goldanskii, V.; Makarov, D.; *Chem.Phys.* **1991**, *154*, 407. (d) Benderskii,
V.; Makarov, D.; Pasture, D. *Chem.Phys.* **1992**, *161*, 51. (e) Benderskii, V.;
Makarov, D.; Grinevich, P.; *Chem. Phys.* **1993**, *170*, 275. (f) Benderskii,
V.; Makarov, D.; Wight, C. Adv. *Chem. Phys.* **1994**, *88*, 1.

(37) Shida, N.; Barbara, P. F.; Almlöf, J. *J. Phy. Chem.* **1991**, *95*, 10457.

(38) Barnes, G. L.; Sibert III, E. L. *J. Chem. Phys.* **2008,** *129***,** 164317.

(39) Carrington, T. Jr and Miller, W. H. *J. Chem. Phys.* **1986**, *84*, 4364.

(40) Makri, N.; Miller, W. H. *J. Chem. Phys.* 1989, 91, 4026.

(41) Shida, N, Barbara, P. F. Almöf, J. E. *J. Chem. Phys.* **1989**, *91*, 4061.

(42) Yagi, K.; Taketsugu, T.; Hirao, K. *J. Chem. Phys.* **2001**, *115*, 10647.

(43) Tew, D. P.; Handy, N. C. *J. Chem. Phys.* **2006**, *125*, 1084313.

(44) Tauterman, C. S.; Voegele, A. F.; Loerting, T.; Liedl, K. R. *J. Chem. Phys.*
2002, *117, 1962*.

(45) Coutinho-Neto, M. D.; Viel, A.; Manthe, U. *J. Chem. Phys.* **2004**, *121*,
9207.

(46) Wang, Y.; Braams, B.; Bowman, J. M.; Carter, S.; Tew, D. P. *J. Chem. Phys.*
    2008, *128*, 224314.

(47) Verner, M. V.; Scheiner, S. *J. Chem. Phys.* **1994**, *101*, 9755.

(48) Giese, K.; Künh, O. *J. Chem. Phys.* **2005**, *123*, 054315.

(49) Gil, M.; Waluk, J. **2007**, *129*, 1335.

(50) Sarai, A. *Chem. Phys. Lett* **1981**, *83*, 50.

CHAPTER 2

COMPUTATIONAL METHODOLOGY

2.1 INTRODUCTION

Computational chemistry is a branch of theoretical chemistry where the primary focus is solving chemical problems *in silico* that is by computations. There are four steps involved here

      1. Definition of the problem,

      2. Method of solution,

      3. Level of theory to be used,

      4. Running the program.

In the first step one defines the problem of interest from a computational perspective. In the second step one defines the sequence of computations that will provide the answers to the questions framed in the first step. Most of the problems of practical nature do not have solutions of closed form. Consequently,

one must to resort to approximations of different levels of accuracy. The choice of such approximations forms the third step. Most of the computations require extensive coding of the theories involved. This part of is carried out by using standard block box programs. This is the fourth step.

The problem that we intend to address in the present thesis requires the description of the reaction path in the proton transfer reactions and the origin of the reduction in the barrier to such a process in terms of the changes in the underlying electronic structure induced by the motion along the promoter modes. In the next section we describe the available electronic structure theories and the particular approach that we use. In section 3 we discuss the tools of analysis that we use. These are the intrinsic reaction co-ordinate (IRC), the natural bond orbital analysis (NBO) and population analysis. Finally, we have used Gaussian-03 suit of programs for all our calculations[1].

2.2 METHODS

Since our problem is regarding the variation of barrier height, we use quantum chemical electronic structure theory for our calculations. Within the Born-Oppenheimer approximation, the nuclei move under the influence of the electronic energy (The eigen value of the electronic Hamiltonian at that nuclear configuration). To that extent one has to solve the time independent electronic Schrödinger equation. There are, essentially, two classes of methods to solve the

electronic Schrödinger equation. These are the wave function based methods, and the density functional theoretic approaches.

The wave function based methods expand the wave function in a suitable basis. The most common approximation in this approach, is the Hatree-Fock (HF) approximation. In this, the wave function is representing as a single Slater determinant for closed shell molecular systems and the energy is obtained by the Ritz variational principle[2]. For several applications the HF approximation is inadequate. This is primarily because the correlation energy (E_{NR}-E_{HF}) is roughly of the same order of magnitude as the various difference energies, such as the reaction energy. Consequently, the HF approximation does not estimate them properly. There are three approaches to go beyond HF approximation. The first of them is the configuration interaction method (CI) and its various variants such as the complete active space self consistent field (CASSCF) procedure. These methods depend on the Ritz variational principle to provide the working equations. Some of the approximations in this approach, such as, the limited CI with doubles, are not size consistent.

The second approach is the use of perturbation theory. The many body perturbation theory with Møller-Plesset (MP) partitioning of the Hamiltonian is a size consistent theory at all orders. However, a limitation of this approach is that the underlying wave function is not properly defined.

The third approach is the coupled cluster (CC) method. Here, one represents the wave operator that maps the unperturbed reference wave function

to the exact wave function by an exponential ansatz. The method is size consistent and highly accurate. However, it is computationally quite demanding.

The density functional theories start from the Hohenberg-Kohn theorem. This theorem states that there exists a one to one correspondence between the electronic density of the system and its energy. Thus, if one can determine the electron density and find the universal functional that relates the density and the energy, one can determine the ground state energy directly from the density. The problem however, is to ensure that the underlying wave function satisfies the N-representability conditions. Kohn and Sham solved this problem by suggesting that the wave function be represented as a Slater determinant of N orbitals and writing the total electronic density as a sum of the individual densities from each orbital. Once this is done, the total energy of electronic system can be written as the sum of individual densities of all the occupied orbitals. Once this is done, the total energy can be written as,

$$E_{DFT}[\rho] = T[\rho] + E_{ne}[\rho] + J[\rho] + E_{xc}[\rho] \tag{2.1}$$

at this point the second problem of density functional theory makes its appearance. The exchange correlation functional $E_{xc}[\rho]$ is not known. This has to be approximated. Commonly, it is split in to two parts, $E_x[\rho]$ and $E_c[\rho]$. The $E_x[\rho]$ is normally approximated by a local density approximation or by some variant of gradient corrected methods. One of the most popular approximations is due to Becke[3]. The correlation functional is similarly fitted, a popular functional of this category is due to Lee-Yang-Paar[3]. We have used the B3LYP functional through out our work.

The DFT is deficient in describing the dispersion contributions to the total energy and consequently, underestimates the barrier heights for proton transfer reactions when used in conjunction with B3LYP functional. Our own goal is to analyze the changes in the wave functions along the intrinsic reaction co-ordinate rather than actual energy differences. To that extent, we have opted to use B3LYP functional. Since, the B3LYP approach is based on Kohn-Sham philosophy it requires a basis set. We have used the aug-cc-pVTZ through out our calculations. This basis set is known to provide adequate description of this class of systems[4].

2.3 TOOLS OF ANALYSIS

The first step in our analysis is the definition of the reaction path. It provides the details of the nuclear motion from the reactant to the product. Several such reaction paths have been discussed in literature. The minimum energy path (MEP)[5] the maximum probability path (MPP)[6], the expectation value path (EVP)[6] are some examples. To be sure, the reactive flux does not follow any single path due to the uncertainty principle; rather a reaction path is indicative of the region of the potential energy surface over which most of the reactive flux occurs. Out of the several possible options the MEP is the simplest and the easiest to obtain computationally. It is defined as the path that follows the steepest gradient at every point from the transition state in mass weighted Cartesian co-ordinates. In a very general sense it may be defined as the path downward from the saddle point

to the minima on either side by a particle whose velocity is infinitely damped. The calculation of such a path requires the details of the potential energy surface alone. In contrast, the other paths such as MPP and EVP require the calculation of the vibrational states on the PES. Defined in terms of the mass weighted Cartesian co-ordinates, the MEP is called the intrinsic reaction co-ordinate (IRC). We have calculated the IRC for all our systems as implemented in the Gaussian-03 suit of programs.

The second tool we use is the Natural Bond Orbital (NBO) analysis[7]. The natural bond orbital analysis is a convenient tool to analyze the electronic structure in terms of chemically significant Lewis structures. The analysis is developed from the concept of natural orbitals of the many electron systems. Natural orbitals (NO) are defined as a set of orbitals that diagonalize the single particle reduced density matrix of system concerned. One can write the single particle reduced density matrix for all the orbitals centered on a given atom in the molecule. This forms, one sub block along the diagonal of the full single particle reduced matrix. Ignoring its coupling to other sub blocks one diagonalizes it to obtain natural atomic orbitals (NAO). Obviously the NAO`s centered on one atom are not orthogonal to the NAO`s centered on another atom. So, these individual groups of NAO`s are orthonormalized. From these orthonormalized NAO`s the core (orbitals with occupancy = 2) and Rydberg (those with occupancy = 0) are deleted. All possible pairs of atoms are now considered. Each 2×2 sub block, corresponding to every pair of atoms in the molecule, of the density matrix

is considered from which the core and lone pair contributions have been removed. The eigenfunctions of these projected reduced density matrices are the natural bond orbitals. The eigenvalues represent the populations in the concerned natural bond orbitals. If necessary, one might go beyond the collection of pairs of atoms, for example to describe three center bonds. For most of the systems that one encounters in organic chemistry, such higher order analysis is not required.

Finally, the charges on the various atoms in a molecule are obtained through population analysis. There are several approaches to calculate the charge on an atom in a molecule. The Mulliken population analysis, methods based on electrostatic potential, and, electron density, are some of the methods. Indeed, there is no unique way of defining the charge on an atom in a molecule, because the orbitals on different atoms overlap significantly. We have used the simplest of these techniques, the Mulliken population analysis. In this approach the net charge on atom A is given by,

$$q_A = Z_A - \rho_A, \tag{2.2}$$

where Z_A is the atomic number and ρ_A is the electronic charge on that atom. It is computed as

$$\rho_A = \sum_{\alpha \in A} \sum_{\beta} D_{\alpha\beta} S_{\alpha\beta}. \tag{2.3}$$

Here, S is the overlap matrix and D is the single particle reduced density matrix in atomic orbital representation given by

$$D_{\alpha\beta} = \sum_{j \in occMO's} C_{\alpha j} C_{\beta j}. \tag{2.4}$$

The matrix *C* represents the co-efficient matrix atomic orbitals in the molecular orbitals. Finally, we have used the Gaussian suite of programs (G03, E. 0. 1) for all our calculations.

REFERENCES

(1) Frisch, M. J. *et al*. *GAUSSIAN 03*; Gaussian, Inc.: Pittsburgh, PA, **2003**.

(2) Jenson, F. *Introduction to computational chemistry* Wiley: New York, **2007**.

(3) Murrell, J. N.; Kettle, S. F. A.; Tedder, J. M. *Valence theorey*, New York, **1970**.

(4) Chocholoušová, J.; Spirko, V.; Hobza, P. *Phys. Chem. Chem. Phys.* **2004**, 6, 37.

(5) Fukui, K. *Acc. Chem. Res.* **1981,** *14,* 363.

(6) Shida, N, Barbara, P. F. Almöf, J. E. *J. Chem. Phys.* **1989**, *91*, 4061.

(7) Cramer, C. J. *Essentials of Computational Theories and Models* Wiley: New York, **2007**.

CHAPTER 3

NATURE OF ELECTRON FLOW ALONG THE IRC DURING PROTON TRANSFER

3.1 INTRODUCTION

Our goal in the present study is to test the hypothesis that the promoter mode enhances the propensity of the delocalization of the lone pair of electrons on the acceptor atom into the antibonding σ^* orbital of the bond between hydrogen and donor atoms, and, as a consequence, brings down the Donor-hydrogen covalent bond. This brings about a reduction in the barrier to proton

transfer. To this end we analyze the changes in the electronic structure along the IRC in two proto-typical hydrogen transfer reaction systems, cyclic $(HF)_3$ and formic acid dimer in this chapter. Both the systems undergo concerted multiple proton transfer. However, the two systems differ considerably in the degree of complexity that they display. The $(HF)_3$ has only σ bonds. All the three protons move simultaneously from their source to the target atoms. The three fluorine atoms act both as proton acceptors and donors. All the vibrations in the system are effected in this process. The dynamics of proton transfer in the formic acid dimer is, on the other hand, more intricate. The donor and acceptor atoms are distinctly separate. The OCO groups undergo a displacement along the asymmetric stretch from one equilibrium position to the other during the proton transfer. This leads to a reorganization of the π electron network. Finally the C-H group remains (at least to zeroth order) as a spectator to the hydrogen transfer. These additional features make the system more complex. Not withstanding this increased degree of complexity in FAD, the essential changes in the electronic structure along the IRC are similar in the both the systems.

The intrinsic reaction coordinate is the path of steepest descent from the transition state to the reactant and product in mass-weighted Cartesian co-ordinates[1]. The nuclear wave packets are unlikely to follow the IRC strictly during the chemical reaction due to residual momentum along different directions, and, tunneling effects. Alternatives to IRC such as the optimal tunneling path have been suggested in the literature to incorporate such effects[2, 3]. However, the

IRC is the simplest path that can be obtained without a detailed analysis of the dynamics and provides an adequate description of the features of the potential surface that control the overall dynamics[4].

We begin our analysis with a summary of the nature of the IRC of the two test systems. Sibert and coworkers[5] identified three modes that are essential for a reduced dimension description of the reaction surface. The first of these is the symmetric OH stretch at the TS. This is essentially the proton transfer coordinate. The second is the dimer stretch mode. As can be seen from Fig.1 of Ref. 5, this mode essentially modulates the effective barrier height to the proton transfer and is symmetrically coupled to the proton transfer coordinate. Thus, it satisfies the Cui–Karplus criteria for the promoter mode. The third mode is the symmetric dimer rock mode. From Fig. 1 of Ref. 5 it is apparent that it is antisymmetrically coupled to the proton transfer coordinate. As a consequence, it undergoes a net displacement from the reactant to the product. The proton exchange in FAD is accompanied by the reorganization of the π-network in which one pair of CO π-bonds are broken and another pair is formed. The consequent changes in the bond lengths require a readjustment of the heavy atoms. The dimer rocking mode and the OCO asymmetric stretch are affected in this process. So, they are part of the overall reaction coordinate, in addition to the proton transfer coordinate. In an earlier work, Loerting and Liedl[6] analyzed the IRC in terms of the normal modes of the TS (Fig. 3 of Ref. 6). They identified the four modes that are mainly involved in the IRC of the proton transfer reactions. In addition to the three

identified by Sibert and coworkers[5] they suggested the CO_2 bending mode as well. From Fig. 3 of Ref. 7, it appears as if this mode is also symmetrically coupled to the proton transfer coordinate. However, the net displacement in this coordinate is much smaller than the dimer stretch. Thus, of the four important modes that undergo large amplitude motion, the dimer stretch plays the role of promoter mode to a major extent and the CO_2 bend to a lesser extent. Note that, both these modes bring the acceptor oxygens closer to the migrating hydrogen atoms. This statement might look a little odd in view of the data of Ref. 9. Sibert and coworkers[9] found tunneling splitting increases as the symmetric dimer rock is excited, relative to the ground state. Since it is antisymmetrically coupled to the proton transfer coordinate and excitation in it enhance the tunneling rates, this mode qualifies to be a demoter mode in the Cui–Karplus classification. The enhanced splitting in the excited states of this mode relative to the coupled ground state is consistent with the conclusions of Cui and Karplus[8].

Liedl et. al[9] analyzed the nature of the three modes that are necessary to take the C_{nh} structures of $(HF)_n$ clusters at equilibrium geometry to the corresponding D_{nh} transition states. These are the symmetric HF stretch that eventually leads to the proton transfer, the symmetric FF stretch and the symmetric HF bending modes both in the C_{nh} and the D_{nh} geometries. They found that the tunneling path that starts from C_{nh} structure follows the nearly flat valley corresponding to the FF stretch, and near the TS turns in the direction of the HF stretch. They also noted that the movement along the HF bend direction is rather small. From the model

potential surface that they have fitted for these two modes (Fig. 4 of Ref. 9), it is apparent that the FF stretch is symmetrically coupled to the proton transfer coordinate, HF stretch. Thus the symmetric FF stretch is the major promoter mode for this system according to the Cui–Karplus analysis.

Instead of the normal modes at the TS, we use the average distance between the heavy atoms that are exchanging the proton as a measure of the displacement along the promoter mode. We define q_{DA} by

$$q_{DA} = R_{DA} - R_{DA}^{\ddagger},$$ (3.1)

where R_{DA} is the average distance between the donor and corresponding acceptor atoms at that point on the IRC. In $(HF)_3$ for example, it is the average of the three F-F distances

since all the three fluorine atoms act as both proton donors and acceptors. Similarly $R_{DA}^{\ddagger}$ is the average distance between the donor and acceptor atoms at the TS. We present q_{DA} against the IRC in Fig 3.1. The average distance between the donor and acceptor atoms shows three distinct regions. In the first region where IRC is less than −0.5, q_{DA} decreases almost linearly from about 0.25 Å to 0. On the other side of the transition state where IRC is greater than +0.5, it increases almost linearly from 0 to 0.25Å. In the intermediate region, around the transition state, the donor acceptor distance remains constant. In Fig. 3.2 we present the effective displacement of hydrogen atom defined by

$$q_{DH} = R_{DH} - R_{DH}^{\ddagger} - \frac{q_{DA}}{2},$$ (3.2)

Fig. 3.1: The average distance between donor and acceptor atoms along the IRC in FAD ($——$) and $(HF)_3$ ($– \bullet –$).
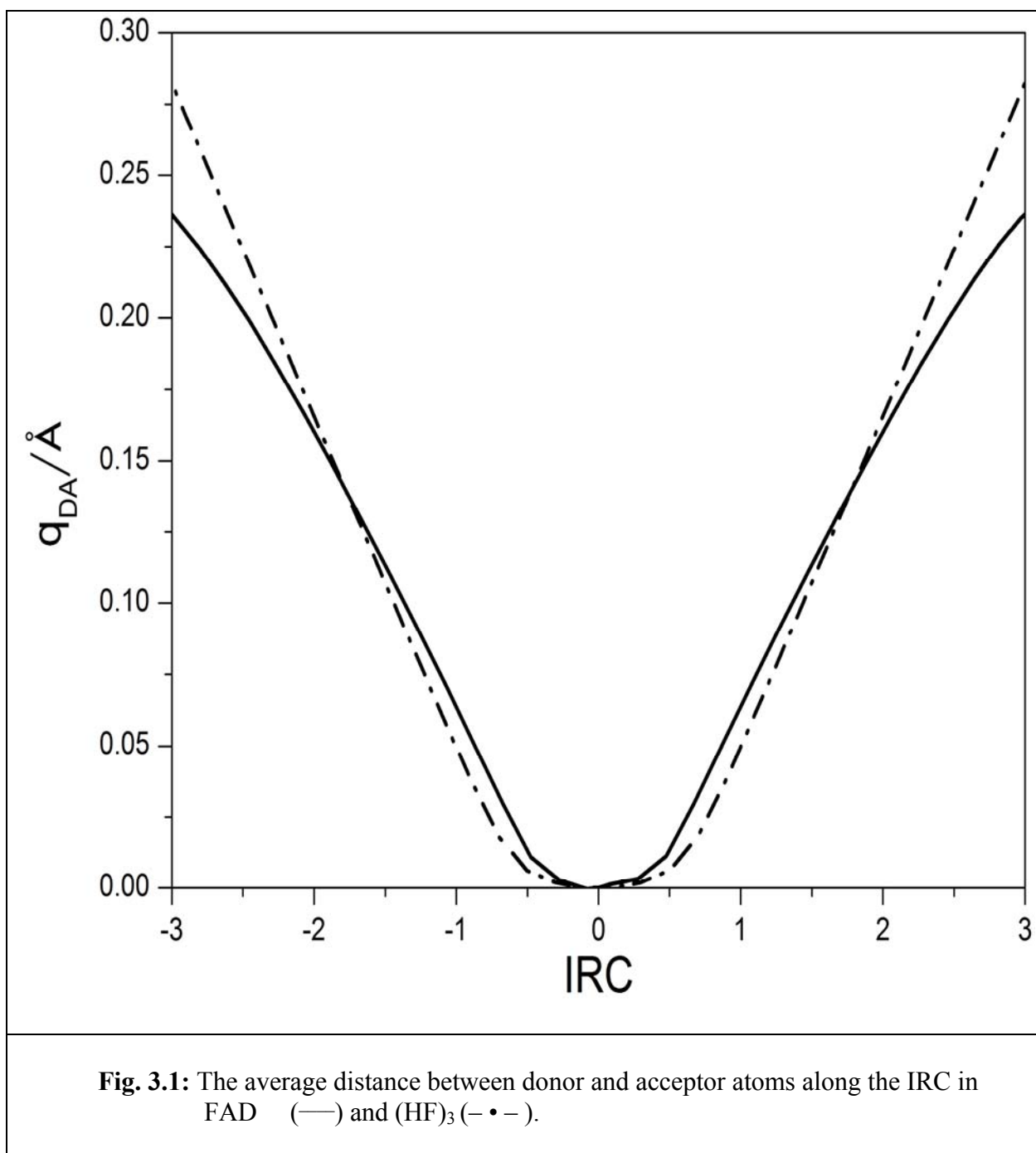
where R_{DH} is the average distance of the hydrogen atom from the donor atom defined analogous to R_{DH} and $R_{DH}^{\ddagger}$ is the hydrogen-donor separation at the TS. Note that as the heavy atoms move, in the dimer stretch of FAD for example, they carry the much lighter proton along with them. To eliminate this component from the proton motion, we subtract $\dfrac{q_{DA}}{2}$ from the distance traveled by the proton in Eq. 3.2. Again the curve shows three distinct regions. In the first region where the IRC is less than −0.5, the change in the q_{DH} is rather small. In the second region around the transition state q_{DH} goes through a major change of almost 0.4 Å. These changes are better appreciated in terms the slopes of curves. The q_{DH} for FAD is –0.32, –0.15 and 0.0 at IRC = –3.0 and –0.5 and 0.0 respectively. Thus the slope of the curve is close to 0.07 in the first region and 0.3 in the second region. Though the total changes in q_{DH} are comparable in both the regions, the displacements they require for this change along the IRC are quite different. The two curves show clearly that the reaction path takes a sharp turn at IRC ≈ ±0.5. The two extreme regions are the dominated by the motion of the heavier atoms while the middle region consists of essentially the proton motion. This feature of the IRC in the proton transfer reactions was noted earlier by Liedl and coworkers[9,10].

Fig. 3.2: The average distance traveled by the hydrogen atom(Eq.3.2) from the donor atom in FAD(——) , (HF)$_3$ (– • –).
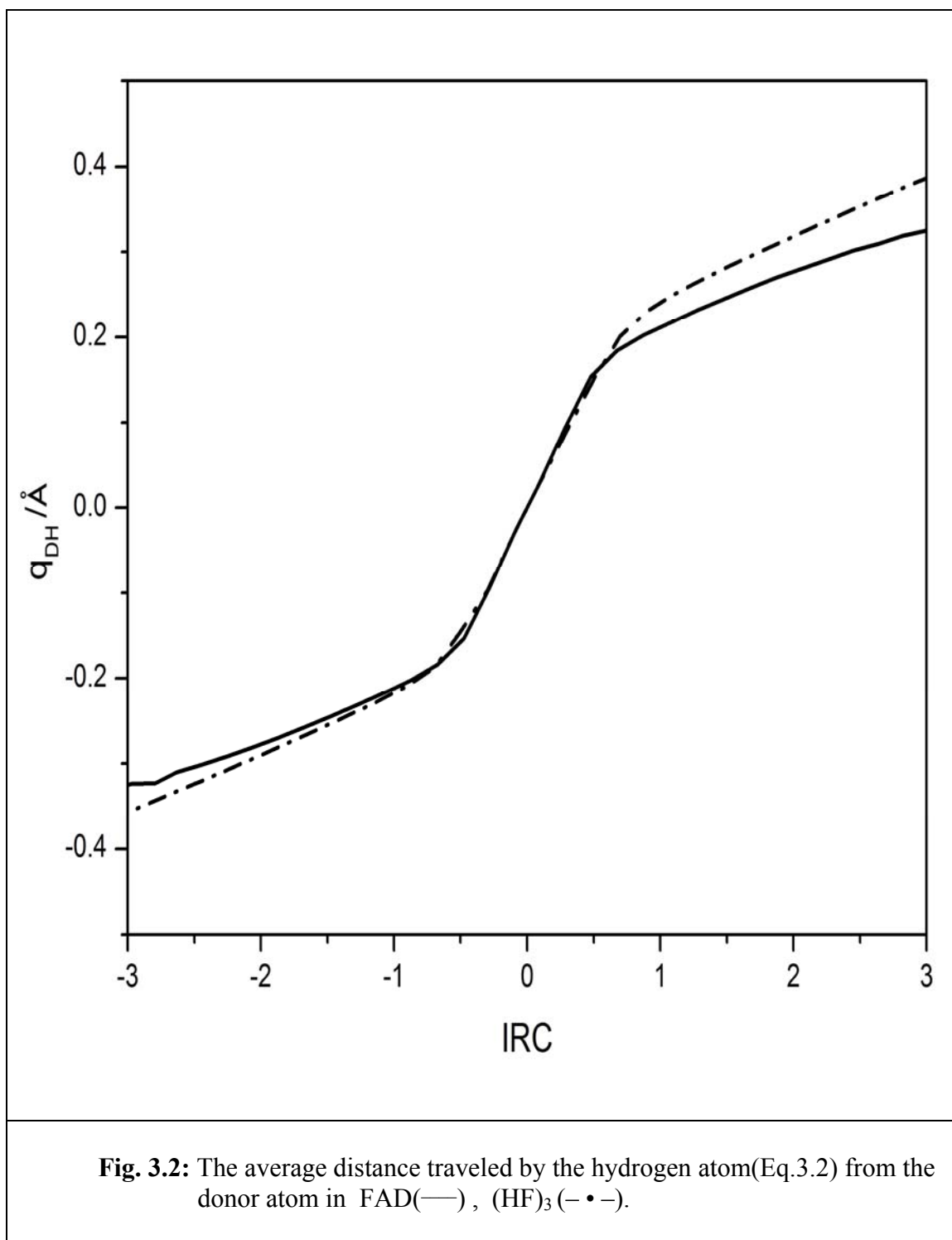
3.2 ELECTRON PAIR DELOCALIZATION

We next turn to the implications of the heavy atom motion in the first region of the IRC. Note that though the q_{DH} changes very little in this region (Fig. 3.2), the hydrogen atom still moves a considerable distance towards the acceptor, because, it is carried along by the donor atom in the first region of the IRC. This brings the 1s orbital of hydrogen into a closer proximity with the lone pair orbital located on the acceptor atom as the two centers approach each other. Given the large disparity in the electronegativities of donor atom and hydrogen atom, the antibonding (σ^*) orbital of the donor-hydrogen covalent bond has a predominantly hydrogen 1s orbital character. This orbital develops a significant overlap with the lone pair orbital on the acceptor as the two heavy atoms approach each other. This enhances the coupling between these two orbitals, thus facilitating the delocalization of the lone pair electrons into the σ^* orbital. We present the variation of population in the σ^* orbital of the donor-hydrogen bond, and, the number of electrons lost from the lone pair ($2 - N(n_\sigma)$, where $N(n_\sigma)$ is the population in the lone pair orbital) of the acceptor atom along the IRC in Fig. 3.3 As can be seen from the figure, both quantities are practically identical for $(HF)_3$. The population in the $\sigma^*(HF)$ orbital is ~0.03 near the reactant geometry (IRC = − 3.0). It rises to ~0.12 at IRC = –0.5.
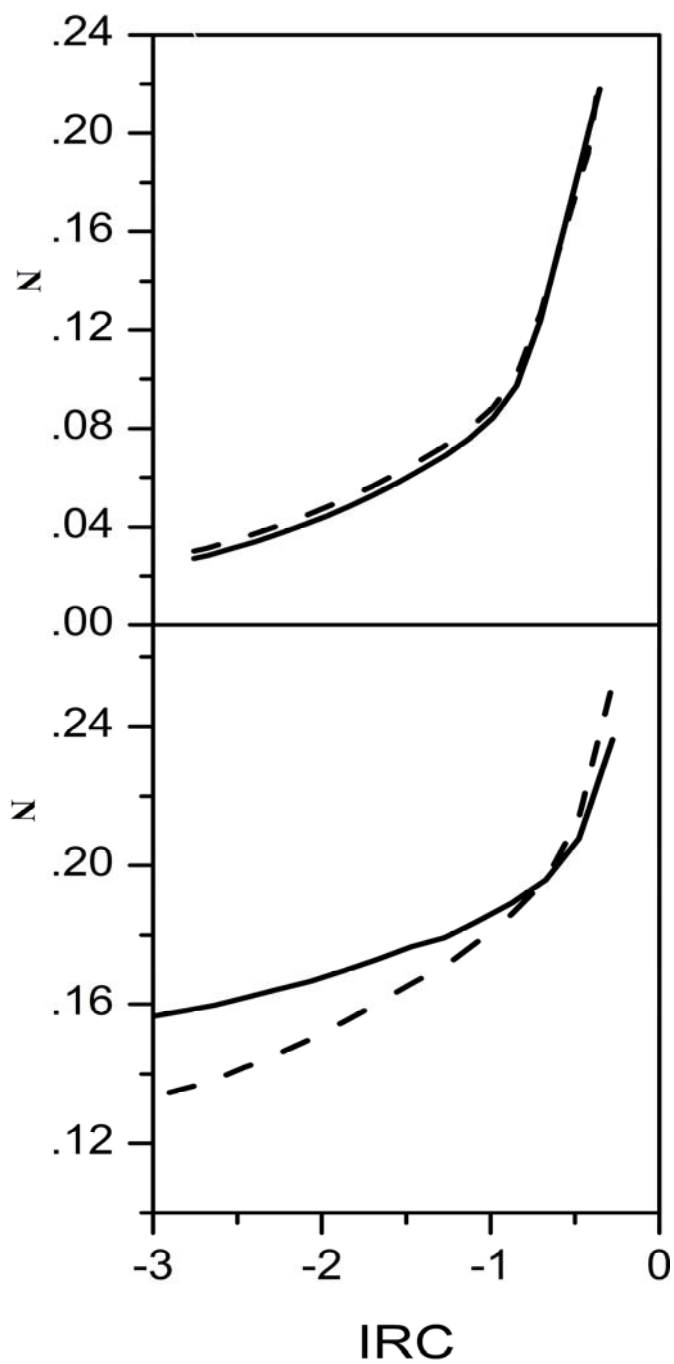
Fig. 3.3a): Variation of the population in the σ*(DH) (——) orbital and the loss of electrons from the lone pair (– – –) orbital on the acceptor atom along the IRC. Upper panel corresponds to $(HF)_3$ and the lower panel corresponds to FAD.
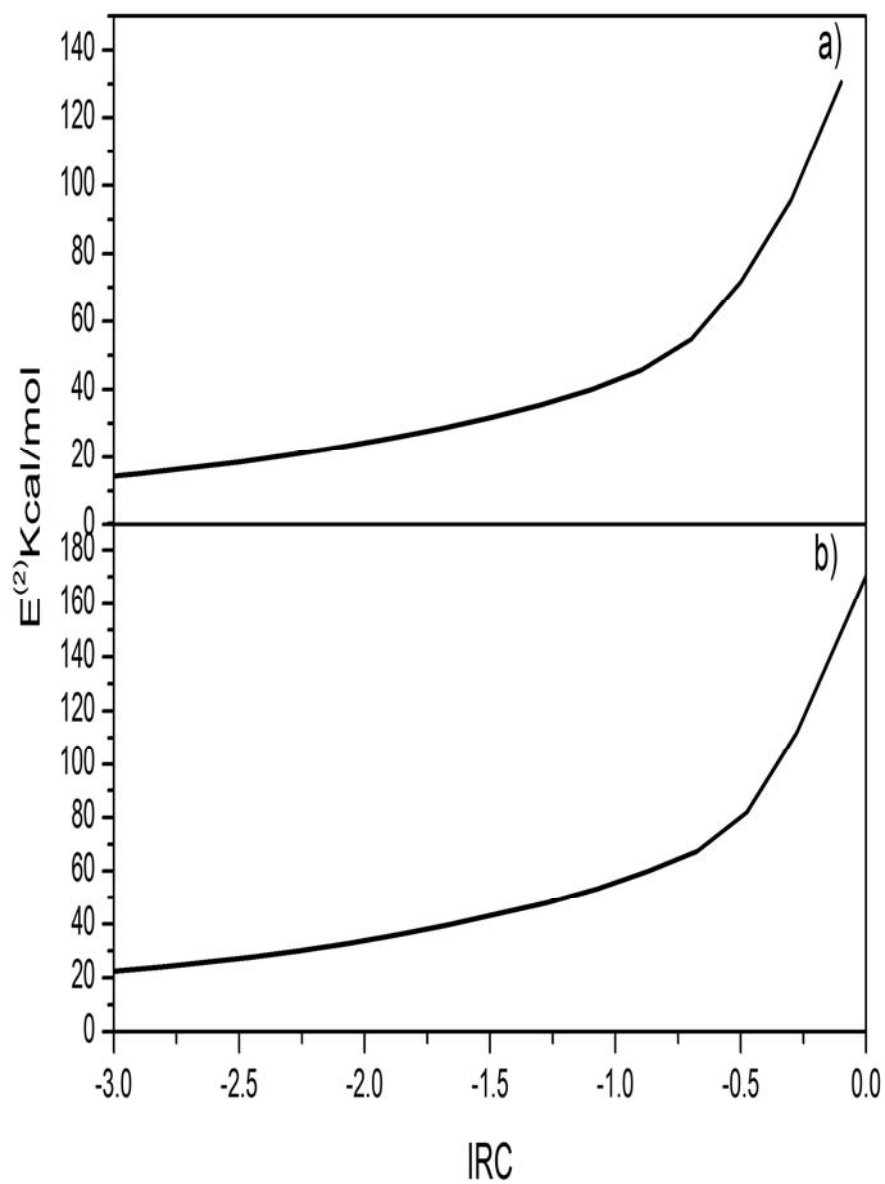
Fig. 3.3b): The second order interaction energy of the σ*(DH) orbital and the lone pair orbital on the acceptor atom along the IRC. Upper panel corresponds to (HF)₃ and the lower panel corresponds to FAD.

So, about 0.09 electrons are transferred in to the σ*(HF) orbital by the time the heavy atom motion stops along the IRC (Fig.3.1). While this number is small, it is still adequate to reduce the strength of the HF bond, and, this lowers the effective barrier to the proton transfer significantly. The electron migration into the σ*(HF) orbital continues beyond IRC = –0.5, though at an accelerated rate. By the time IRC reaches the vicinity of the TS, 0.22 electrons are transferred into the σ*(HF) orbital. As noted earlier, this region of the IRC is dominated by the proton migration from the donor atom. Thus the population changes in this region reflect the actual bond breaking/forming process. The slopes of the curve changes sharply at IRC = –0.5, just as in Figs 3.1 and 3.2. This indicates that the population transfer below IRC = –0.5 is induced by the heavy atom motion, while the population transfer beyond this point on the IRC is the result of the proton migration to its destination. A similar trend is seen in FAD also (Fig.3.3). Here the population in σ*(OH) orbital increases by 0.08e as the IRC increases from IRC = –3.0 to –0.5.

That the population transfer stabilizes the system (and they contributes to the reduction in the barrier), is seen from the second order stabilization energy due to such population transfer. This data is presented in Fig. 3.3b. In the promoter mode dominated region of the IRC, the stabilization energy increases from about 20 kcal/mol to about 60 kcal/mol in FAD and from ~10 kcal/mol to 50 kcal/mol in (HF)$_3$. The increased population in the σ*(DH) reduces the bond strength of the donor-hydrogen covalent bond.
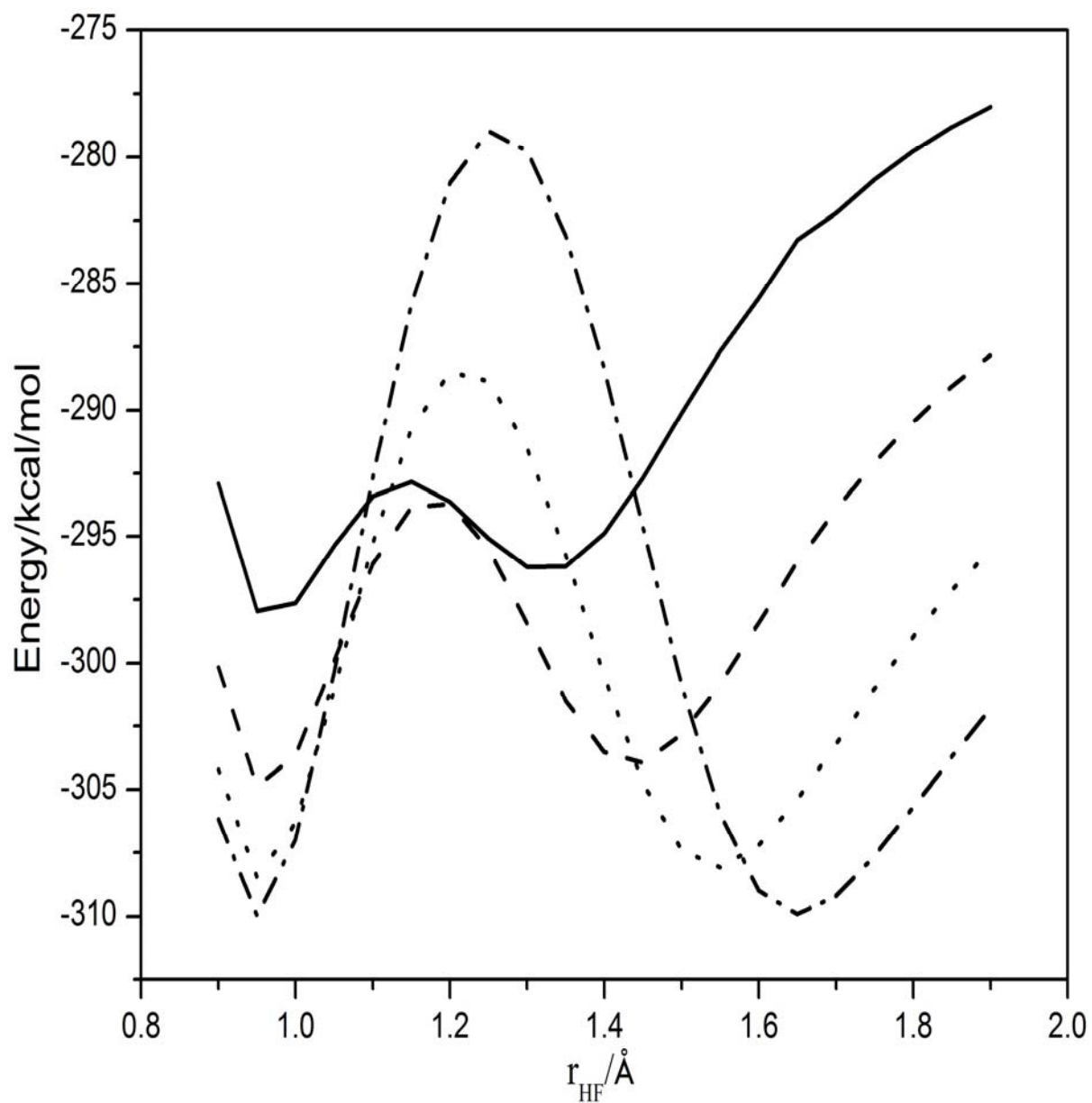
Fig. 3.4: Adiabatic potential energy curves as a function of R_{HF} for fixed values of R_{FF}. $R_{FF} = 2.3A^o$ (——), $R_{FF} = 2.4A^o$ (– – –), $R_{FF} = 2.5A^o$ (• • •), $R_{FF} = 2.6A^o (– • –)$.

In Fig 3.4, we plot the potential along R_{DH} co-ordinate for fixed values of R_{DA} for the $(HF)_3$ system. The reduction in the activation barrier with decreasing R_{DA} values is clearly seen in this figure. Note that in the first part of the proton transfer reaction it is

the R_{DA} which decreases significantly. Thus it is apparent that the role of the heavy atom motion is to bring down the barrier significantly from its value at the equilibrium position by increasing the population in the $\sigma^*(OH)$ orbital. Thus the proton is required to cross over a much smaller barrier.

3.3 VARIATION OF THE VIBRATIONAL FREQUENCIES ALONG THE IRC

One of the immediate consequences of the lone pair delocalization in to the $\sigma^*(DH)$ orbital is on some of the vibrational frequencies of the molecular system. As noted earlier, the increased population in the σ^* orbital decreases the bond strength of the hydrogen-donor covalent bond. Consequently, the force constants associated with stretching vibrations of the hydrogen atom are reduced. In the case of $(HF)_3$ there are three stretching vibrations of the hydrogen atom. The first (symmetric stretch) becomes imaginary at the transition state. The other two, a pair of degenerate stretching vibrations, also feel reduced force constants as the molecule progresses along the IRC. Similarly, in FAD, one of the hydrogen stretching frequencies becomes imaginary at the transition state while the other goes down. The non-imaginary hydrogen stretching frequencies along the IRC
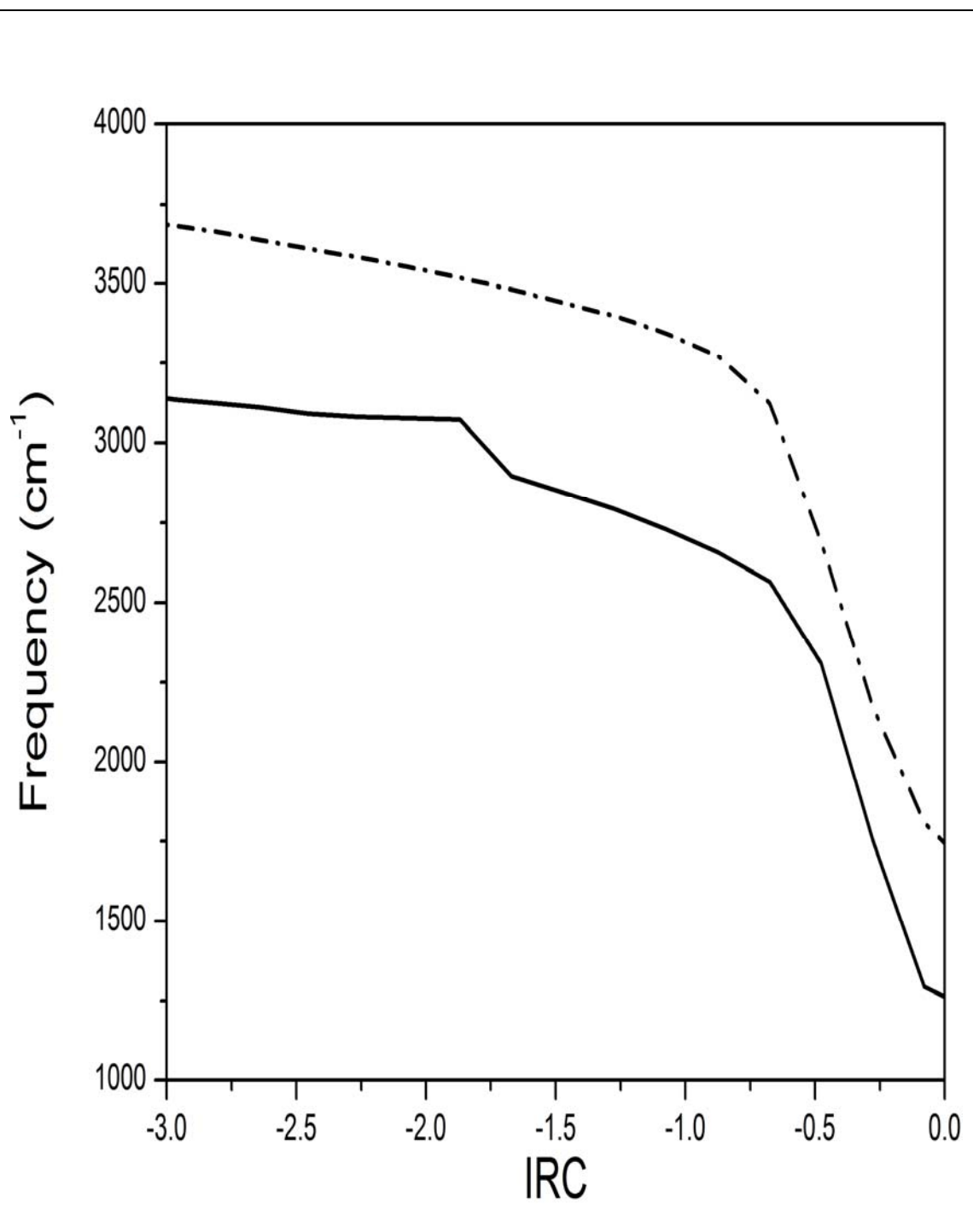
Fig.3.5: Variation of the hydrogen stretching frequencies in FAD (──) and (HF)$_3$ (– • –) along the IRC.

for both the molecules are plotted in Fig. 3.5. As can be seen these two frequencies decrease significantly, by about 1500 cm^{-1}, by the time they reach the transition state. Even at IRC = –0.5, they decrease by ~500 cm^{-1}, reflecting the extent of electron transfer due to the motion along the promoter mode.

The effect of the enhanced population in the σ* orbital has a more complex effect on the bending modes of the migrating protons. While the force constant of the hydrogen-donor bond comes down in this case also, the nascent acceptor-hydrogen bond force constant increases from its near negligible value at the reactant structure. Unlike the situation for the stretch motions where these two bonds oppose each other, both the bonds pull the hydrogen in the same direction if it steps out of the line connecting the donor and acceptor atoms. Given that these two effects oppose each other, it is difficult to predict the variation of the bending frequencies apriori. For the two test molecules we have studied, the bending frequencies actually increase along the IRC. However, the magnitude of this change is quite small, about 200 cm^{-1} on the average. We plot the out of plane bending frequencies of the hydrogen atom of both the molecules in Fig. 3.6 to illustrate this effect. A similar behavior is observed for the inplane bending modes also. The decrease in the stretching frequencies and an increase in the bending frequencies at the transition state relative to the equilibrium structure appear to be a characteristic feature of these systems and had been noted by earlier authors in the literature[11, 12, and 13]. The CH force constants in FAD are not affected by the flow of electrons during the passage of the molecule along the IRC
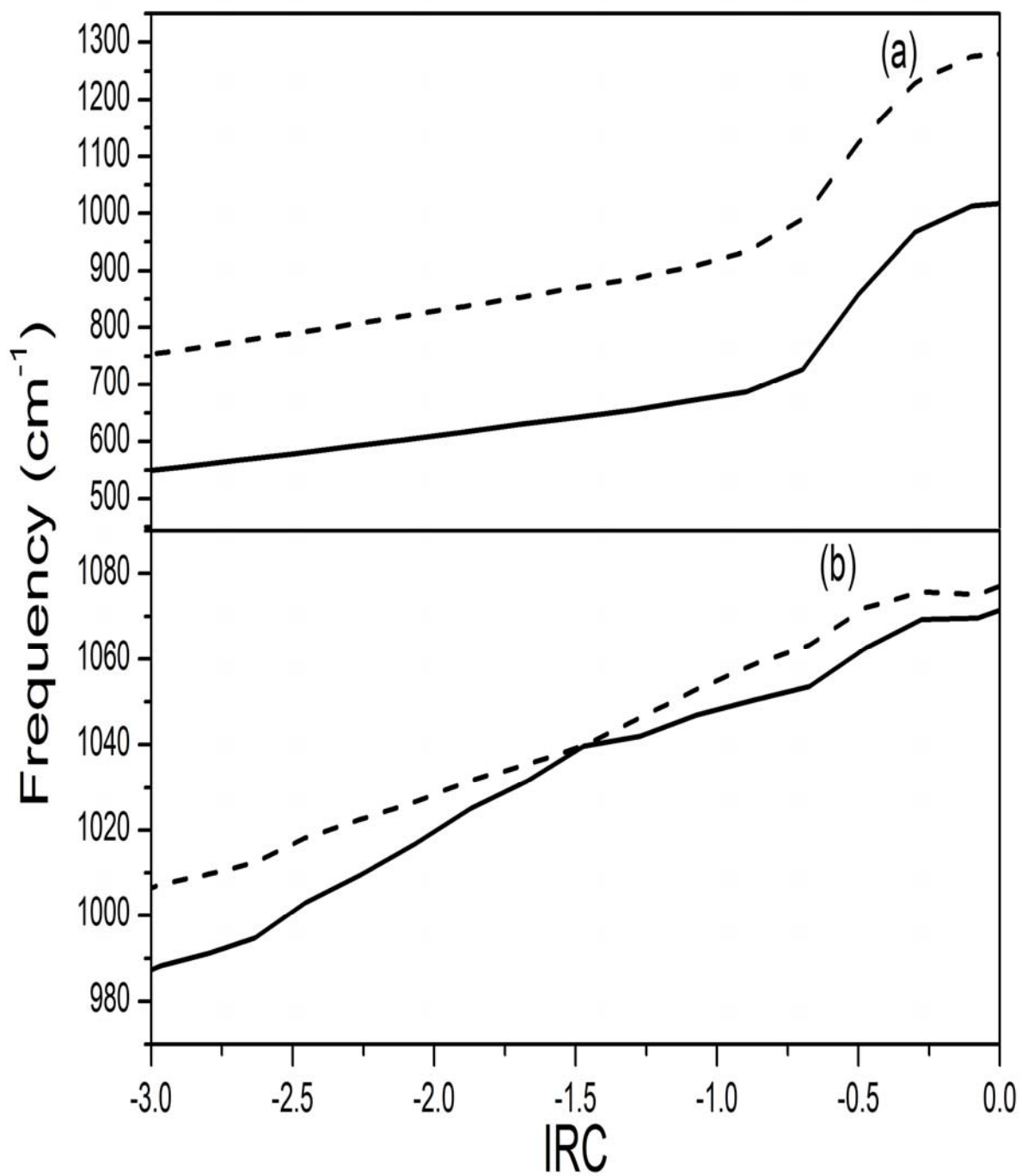
Fig. 3.6: Variation of the out of plane bending frequencies in a) (HF)$_3$ and b) FAD.

described above. Consequently, the frequencies associated with the CH oscillators remain practically unchanged. For example, the symmetric CH stretch frequency varies between 3071 cm^{-1} and 3066 cm^{-1} from reactant to the TS.

3.4 VARIATION OF ATOMIC CHARGES

We next turn to variation of atomic charges along the IRC. As we noted earlier, the σ* orbital is predominantly the hydrogen 1s orbital. Thus, the delocalization of acceptor lone pair in to the σ* orbital should increase the electronic charge density on the hydrogen atom. The Mulliken charge on the hydrogen atom for both the test systems is presented in Fig.3.7. As can be seen, the net charge on the hydrogen atom decreases up to an extent along the IRC, and remain nearly constant thereafter until about IRC ≈ -0.5 when it starts increasing sharply. This again points to the presence of two separate regions in the IRC.

The variation of charge density on the hydrogen atom along the IRC can be understood in terms of a three state four electron model for a single proton transfer between donor and acceptor atoms. Let χ_A , χ_D and χ_H be the orbitals associated with the acceptor, donor and hydrogen atoms respectively. For simplicity we assume that χ_A and χ_D are similar in nature and have the same Fock matrix elements. The 3×3 Fock matrix for the system can be approximated as

$$F = \begin{bmatrix} 0 & f_D & 0 \\ f_D & \Delta & f_A \\ 0 & f_A & 0 \end{bmatrix}, \tag{3.3}$$
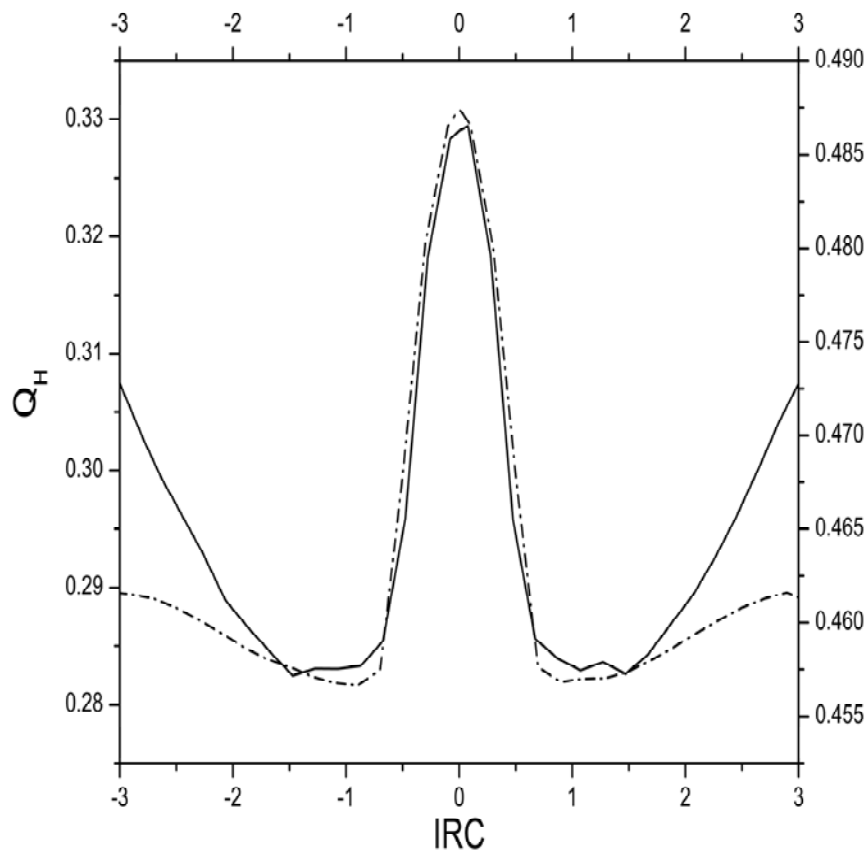
Fig.3.7: Variation of the charge on the migrating hydrogen atoms in FAD (——) and (HF)$_3$ (– • –) along the IRC.

where the orbitals are ordered in the sequence χ_D, χ_H, χ_A.   The scale of the orbital energy is chosen such that the donor and acceptor orbital energies are zero. Δ is the orbital energy of hydrogen orbital, and, in the systems that we are interested in, is expected to be large and positive. We assume that the donor and acceptor orbitals do not interact with each other because of the large separation between them. f_D and f_A are the coupling matrix elements between the donor and acceptor orbitals and hydrogen orbitals respectively. The molecular orbitals of the system are given by the eigenvectors of this matrix. Given the large energy gap, Δ, a first order perturbation treatment should suffice to construct the molecular orbitals. Within this approximation, the molecular orbitals are given by,

$$\Phi_1 = \frac{f_D \chi_D - \left(\frac{f_D^2 + f_A^2}{\Delta} \right) \chi_H + f_A \chi_A}{\sqrt{f_D^2 + f_A^2 + \left(\frac{f_D^2 + f_A^2}{\Delta} \right)^2}} \tag{3.4}$$

$$\Phi_2 = \frac{f_A \chi_D - f_D \chi_A}{\sqrt{f_D^2 + f_A^2}} \tag{3.5}$$

$$\Phi_3 = \chi_H + \frac{f_D \chi_D + f_A \chi_A}{\Delta} \tag{3.6}$$

The corresponding orbital energies are,

$$\varepsilon_1 = \frac{-(f_D^2 + f_A^2)}{\Delta} \tag{3.7}$$

$$\varepsilon_2 = 0 \tag{3.8}$$

$$\varepsilon_3 = \Delta + \frac{f_D^2 + f_A^2}{\Delta} \tag{3.9}$$

Note that the third orbital is essentially the hydrogenic orbital as expected. Up to second order in (f_D/Δ) parameter, the net charge on the hydrogen atom is given by,

$$Q_H = 1 - \frac{f_A^2 + f_D^2}{\Delta^2}$$ (3.10)

We now parameterize the coupling matrix elements f_A and f_D. Since these are essentially electron nuclear attraction terms they must be negative. Their magnitude depends on the separation between the two orbitals. For the 1s orbital this term is known to vary inverse exponentially[14]. In that spirit we parameterize f_A and f_D as,

$$f_A = -V_0 e^{-\alpha R_{AH}} \, ,$$ (3.11)

$$f_D = -V_0 e^{-\alpha R_{DH}} \, .$$ (3.12)

Here V_0 is the strength of the coupling and α is an effective nuclear charge like parameter. Substituting Eq. 3.11 and 3.12 in Eq. 3.10 we finally arrive at ,

$$Q_H = 1 - \frac{2V_0^2}{\Delta^2} e^{-\alpha R_{DA}} \cosh\left[2\alpha \left(R_{DH} - \frac{R_{DA}}{2} \right) \right].$$ (3.13)

We now consider two limiting situations along the IRC. In the earlier part of IRC near the reactants, the movement along IRC is essentially the movement of the donor and acceptor atoms alone. Consequently, in this region R_{DA} decreases noticeably while R_{DH} does not change much. As a consequence, only the exponential term in Eq. 3.13 increases as one progress from reactant towards the transition state. Thus in the early part of the IRC where the movement is essentially along the promoter mode (in this case, R_{DA}) the net charge on

hydrogen atom comes down. Close to the transition state, the IRC is essentially the protonic motion. For the symmetric system we are considering $R_{DH} = R_{DA}/2$ at the transition state. Thus, starting from transition state movement towards reactant or product increases the cosh term, thus, reducing the net charge on the hydrogen atom. This gives rise to the characteristic W shape curve for the charge on the hydrogen atom along the IRC that we see in Fig. 3.7.

3.5 CONCLUDING REMARKS

We have presented an analysis of the changes in the electronic structure along the IRC in two model systems, $(HF)_3$ and FAD. In both cases we find that the IRC is highly curved. In the first part of the IRC it resembles the intermonomer stretch to a significant extent. As the two monomers approach each other, the electrons in the n_σ lone pair on the donor atom oriented towards the hydrogen delocalizes into the antibonding σ^* orbital of the acceptor hydrogen covalent bond. The frequency of intermonomer stretch is quite small, about $240 cm^{-1}$, and remains almost unchanged through out the IRC. The energy required to climb the barrier in this direction is quite small. As the n_σ electrons delocalize the donor-hydrogen bond weakens considerably. The proton migration per se begins when the donor hydrogen covalent bond weakened sufficiently. This occurs at about IRC ≈ -0.5. Thus, in addition to kinematic factors that are inherently present in a heavy–light–heavy system, this change in the magnitude of the gradients in the two directions contributes significantly to the large curvature found in the IRC of these systems.

Such an electron transfer mechanism is possible only in polar hydrogen bonded systems. The σ^* orbital of the existing donor hydrogen bond has a significant contribution from the hydrogen 1s orbital in such systems alone.

The analysis presented in Sec. 3.2 provides us with a criterion to identify promoter modes in proton transfer reactions. As noted in Sec. 3.2, motion along the promoter mode brings down the barrier to proton transfer through enhanced delocalization of lone pair electrons in to the σ^* orbital. Thus, from an electronic structure perspective a promoter mode can be defined as the vibrational mode that promotes the delocalization of the acceptor lone pair of electrons in to the σ^* orbital of the DH covalent bond by bringing about a greater overlap between the $\sigma^*(DH)$ and n_σ (A) orbitals.

Finally, we are left with the π-network reorganization in FAD. We take up this question in the next chapter along with another system malonaldehyde.

REFERENCES

(1) (a) Fukui, K. *Acc. Chem. Res.* **1981,** *14,* 363. (b) Marcus, R. A. *J. Chem. Phys.* **1966**, *45,* 4500. (c) Shavitt, I. *J. Chem. Phys.* **1968,** *49*, 4048. (d) Marcus, R. A. *J. Chem. Phys.* **1968**, *49*, 2610. (e) Truhlar, D. G.; Kupperman, A. *J. Am. Chem. Soc.* **1971**, *93*, 1840. (f) Miller, W. H.; Handy, N. C.; Adams, J. E. *J. Chem. Phys.* **1980**, *72*, 99. (g) Garcia-viloca, M.; Truhlar, D.G.; Gao, J. *Biochemistry*, **2003**, *42*, 13558. (h) Peter, B.; Bell, A.T.; Chakraborty, A. K. *J. Chem. Phys.* **2004**, *121*, 4461.

(2) Shida, N.; Barbara, P. F.; Almlöf, J. *J. Chem. Phys.* **1991**, *94*, 3633.

(3) Tautermann, C. S.; Voegele, A. F.; Loerting, T.; Liedl, K. R. *J. Chem. Phys.* **2002,** *117*, 1962.

(4) Peters, B. *J. Chem. Theory and Compute.* **2010,** *6*, 1447

.(5) (a) Barnes, G. L.; Squires, S. M.; Sibert III, E. L. *J. Phys. Chem.* B **2008**, *112,* 595. (b) Shida, N.; Barbara, P. F.; Almlöf, J. *J. Chem. Phys.* **1991**, *94*, 3633.

(6) Loerting, T.; Liedl, K. R. *J. Am. Chem. Soc.* **1998**, *120*, 12595.

(7) Tautermann, C. S.; Loferer, M. J.; Voegele, A. F.; Liedl. K. R. *J. Chem. Phys*. **2004**, *120*, 11650.

(8) Cui, Q.; Karplus, M. *J. Phys. Chem. B* **2002**, *106*, 7927.

(9) Liedl, K. R.; Kromer, R. T.; Rode, B. M. *Chem. Phys. Lett.* **1995**, *246*, 455.

(10) Loerting, T.; Liedl, K. R. *J. Phys. Chem. A* **1999***, 103,* 9022.

(11) Loerting, T.; Liedl, K. R.; Rode, B. M. *J. Am. Chem. Soc.* **1998**, *120*, 404.

(12) Luckhaus, D. *J. Phys. Chem. A* **2006***, 110,* 3151.

(13) Wang, Y.; Braams, B. J.; Bowman, J. M.; Carter, S.; Tew, D. P. *J. Chem. Phys.* **2008**, *128*, 224314.

(14) Liedl, K. R.; Sekušak, S.; Kroemer, R.T.; Rode, B. M. *J. Phys. Chem. A* **1997**, *101*, 4707.

(15) Murrell, J. N.; Kettle, S. F. A.; Tedder, J. M. *Valence theorey*, New York, 1970.

CHAPTER 4

π-ELECTRON REORGANIZATION DURING PROTON TRANSFER

4.1 INTRODUCTION

As we have seen in the previous chapter, the proton transfer process is assisted by a promoter mode. The promoter mode brings the donor and acceptor atoms closer in such a way that it enhances the propensity of delocalization of the lone pair of the electrons (n_σ) on the acceptor atom into the (vacant) σ^* orbital of the donor-hydrogen covalent bond. As the proton migrates from the donor to the acceptor a charge imbalance is created in the molecule. If the donor and acceptor are connected via π-network the π-bonds reorganize so that the charge imbalance is eliminated. The nature of such π-reorganization is the object of the present

chapter. We analyze the flow of π-electrons in two model systems, FAD and malonaldehyde during the proton transfer.

4.2 THE SYSTEMS

In FAD, the donor and acceptor atoms are distinct in each monomer. The donor has a lone pair of π-electrons, and the acceptor has a π-bond with the carbon atom that lies between the donor and acceptor. As the proton from the second monomer bonds to the acceptor, the π-bond between the acceptor and carbon atom shifts to a π-bond between the carbon and erstwhile donor atom that had lost its proton. On the other hand, in malonaldehyde, the donor and acceptor atoms are separated by two π-bonds; the π-bond between the acceptor and the carbon atom, and the π-bond between the carbons at the α and β position from the donor oxygen atom in addition to the n_π-lonepair on the donor oxygen atom. Thus, three pairs of electrons move in this case in contrast to the situation in FAD, where only two pairs of electrons move during the proton transfer reaction. In that sense, malonaldehyde is a more complex system.

The IRC of malonaldehyde shows clearly the presence of the promoter mode. We present in Fig. 4.1 the distance between the two oxygen atoms as a function of the IRC. Clearly, this variable represents the movement along the promoter mode. In the first part of IRC (< –0.2) the O-O distance decreases by 0.2 Å and again increases to its original value from IRC = 0.2. The distance between the hydrogen
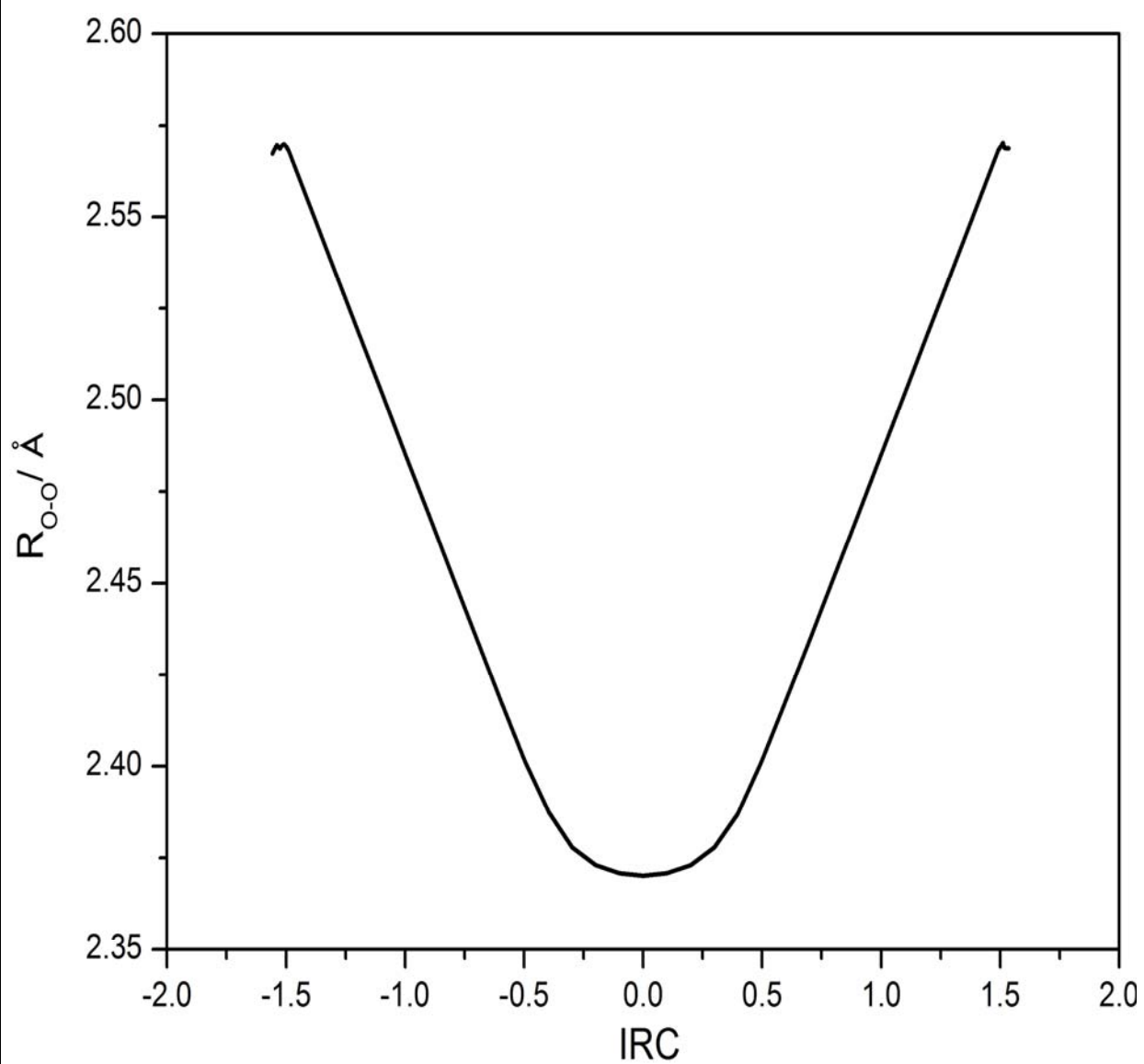
Fig. 4.1: The distance between donor and acceptor atoms along the IRC in malonaldehyde.

Fig. 4.2: The distance traveled by the hydrogen atom from the donor atom in malonaldehyde.
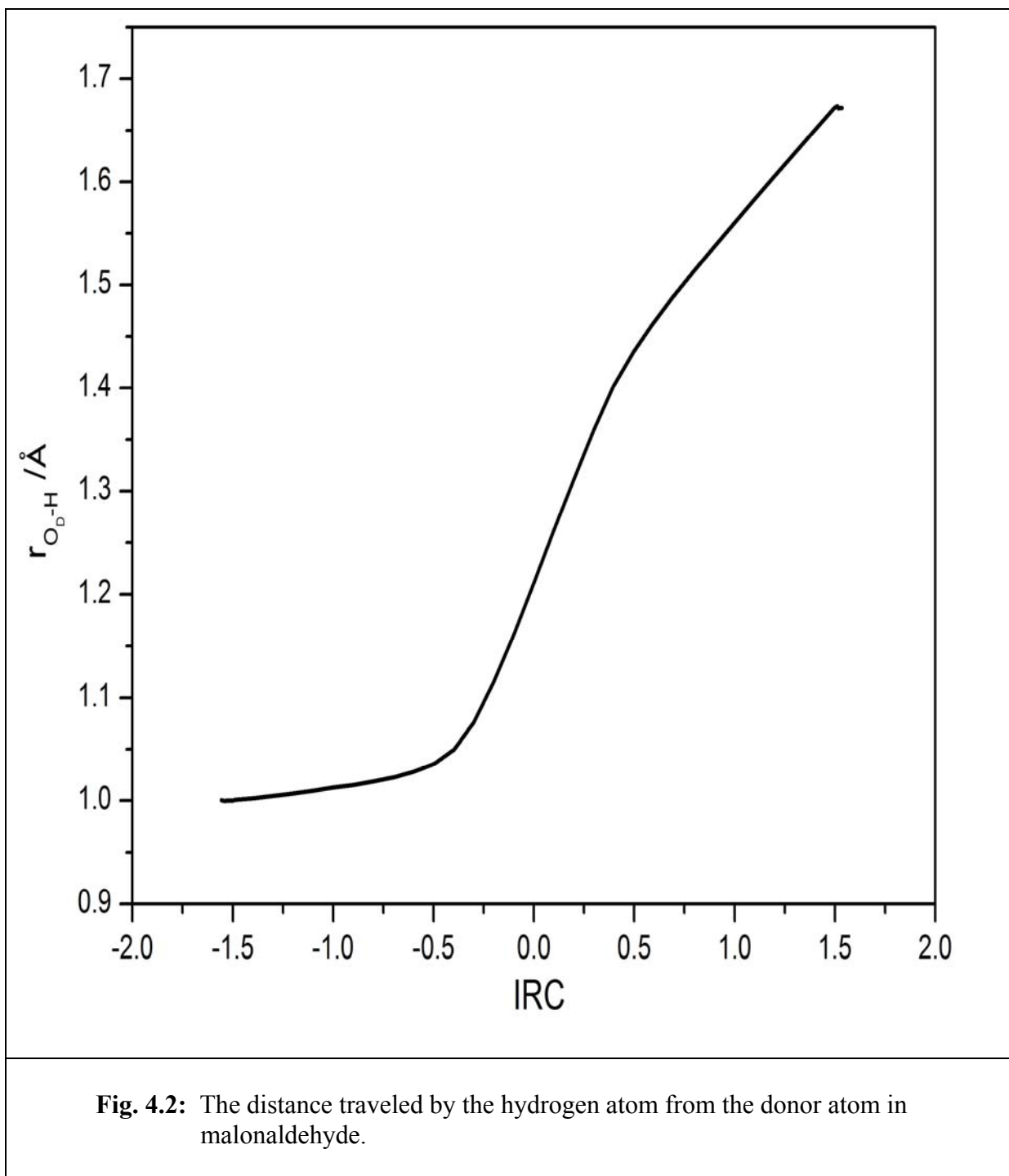
atom and donor atom are shown in Fig. 4.2. Again, in the promoter mode dominated region of IRC, the change in the OH distance is very small. OH distance starts increasing significantly from IRC = –0.2. So, the proton motion begins only after the donor and acceptor approach sufficiently close. The barrier to the proton transfer comes down sufficiently at this point for the proton to start migrating .

We now turn to the specific features associated with OCO rearrangement in FAD. We define the variable q_{co} as

$$q_{co} = r_{c-o} - r_{c=o} \qquad (4.1)$$

This variable represents the displacement along the antisymmetric stretch vibration of the OCO group. We plot q_{co} verses IRC in Fig. 4.3. Upto IRC = –0.5 the changes in q_{co} are small, from about 0.2Å to 0.15Å. Between IRC = ±0.5, q_{co} changes by as much as 0.3 Å. In the rest of the IRC again its variation is small. We recall that this is precisely the interval in which the proton transfer happens. Thus, it is apparent that, at least along the IRC the OCO rearrangement and proton transfer are synchronous. The same reasons that triggered the proton motion also control the OCO rearrangement. So, we have to look at the changes in the electronic structure that can act as a trigger to the OCO rearrangement.
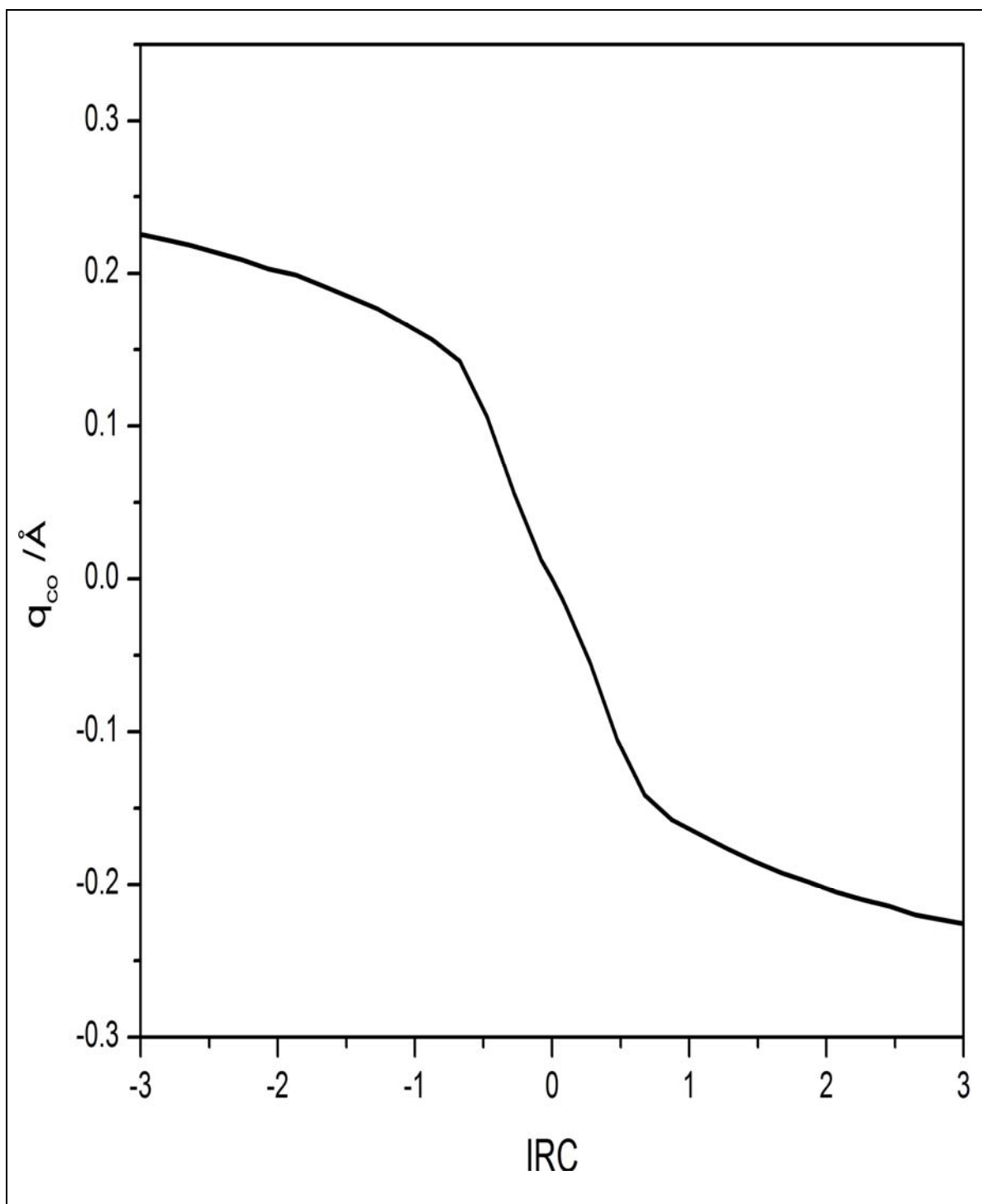
Fig. 4.3: The variation of the antisymmetric q_{co} stretch defined in Eq. 4.1. along the IRC.

4.3 VARIATION OF THE ATOMIC CHARGES ALONG THE IRC

To bring about a π-electron reorganization, some impulse is needed. The trigger for this motion are the changes in the charge of the acceptor atom. We plot in Fig. 4.4 the charges on the donor and acceptor oxygen atoms along the IRC. The charge on the donor remains more or less constant for IRC < –0.5. The major change that is noticeable in this promoter mode dominated regime is the change in the charge of the acceptor oxygen atom. It increases from about – 0.5e at IRC = – 3.0 to about –0.45e at IRC = –0.5. To compensate this loss of charge the acceptor oxygen pulls the π-electrons of the C=O towards itself. Consequently, the π^* (C=O) orbital becomes more localized on the carbon atom. This increases the overlap between the n_π (donor) orbital and the π^* (C=O) orbital. The variation of population in the π^* (C=O) orbital and the number of electrons lost from the n_π orbital $(2–N(n_\pi))$ is shown in Fig. 4.5a. The two numbers match each other very closely. The slope of the curve changes abruptly at around IRC = –0.5 reflecting the change in the character of the IRC near that point. The donation of the n_π electrons of the acceptor into the π^* (C=O) orbital is the first step in the formation of a π-bond between the donor oxygen and carbon atoms as well as the breaking of the existing π-bond between carbon and acceptor atoms. As a consequence of this nascent bond forming/breaking the equilibrium position of the OCO asymmetric stretch shifts from its original position in the reactant towards the new equilibrium position in the product. The stabilization energy due to this electron
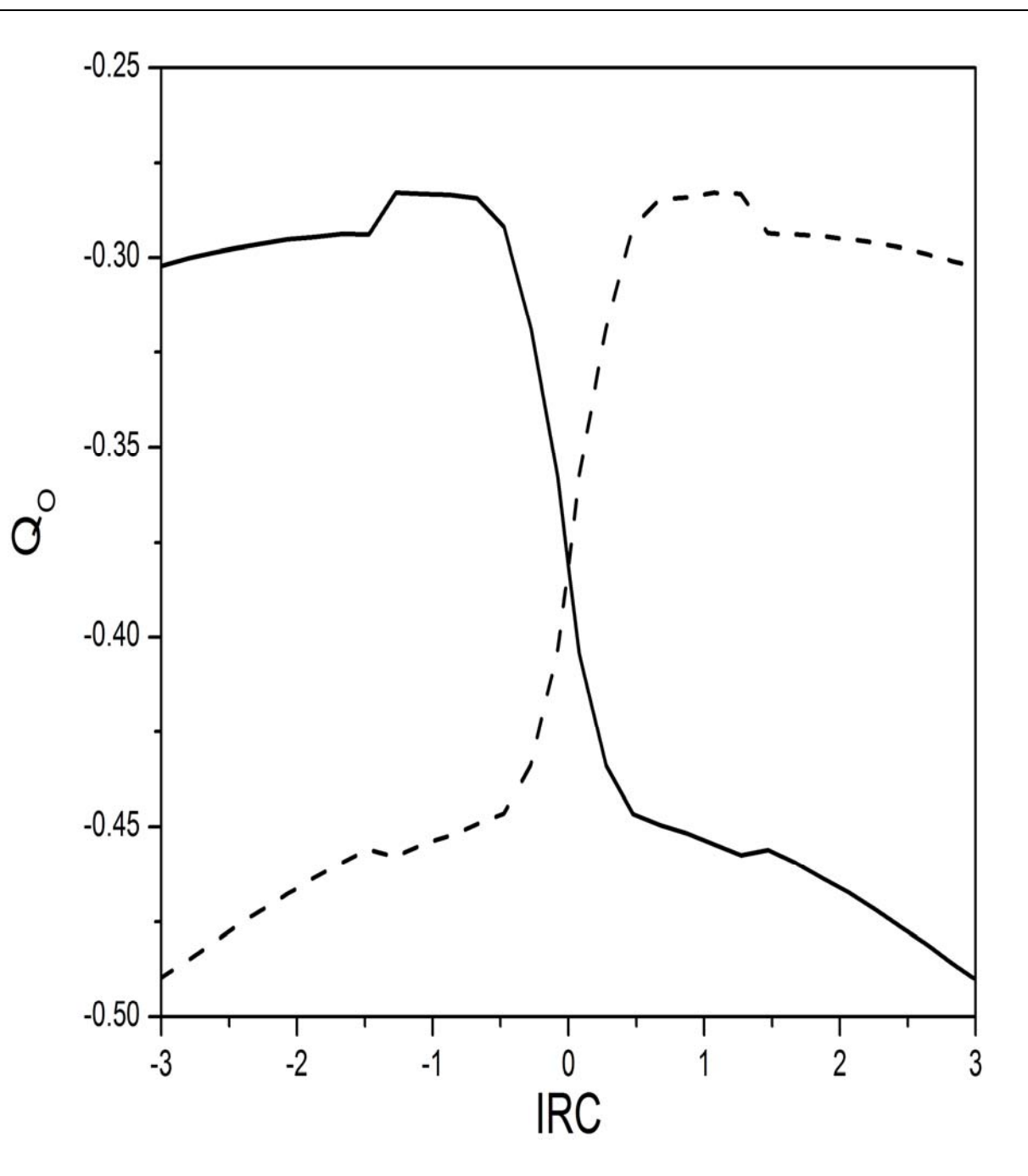
Fig. 4.4: Charges on the donor (——) and acceptor ((– – –) oxygen atoms in FAD.
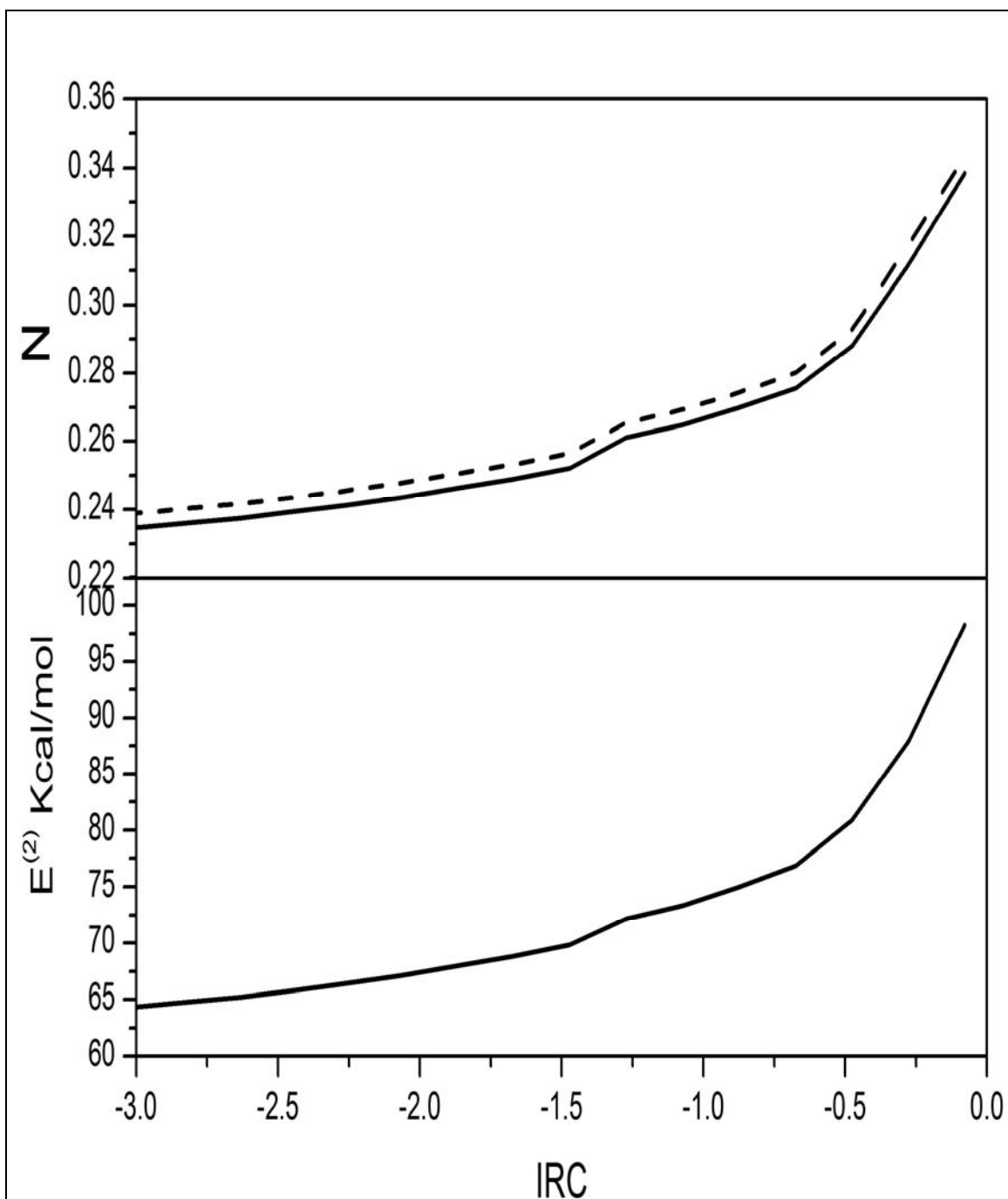
Fig. 4.5: a) The variation of population in π^* (C=O) (——) and the loss of population in the n_π (– – –) orbital of the donor oxygen atom as a function of IRC in FAD. **b)** The interaction energy of the π^*(C=O) and n_π (Acceptor Oxygen lone pair) orbital in FAD.

pair delocalization increases from about 65 kcal/mol to about 75 kcal/mol in the first part of the IRC. It ultimately reaches 100 kcal/mol by the time system reaches the transition state. In contrast, the stabilization energies of the $n_\sigma \rightarrow \sigma^*$ delocalization in FAD (Fig. 3.3b) is about 40 kcal/mol in the promoter mode regime. Thus, the electronic effects from the π network are weaker than the σ-network reorganization. This is to be expected due to the smaller overlaps between the π-orbitals compared to the σ orbitals.

In the second phase of the IRC, the charge on acceptor atom increases sharply from about $-0.45e$ to $-0.3e$, and the charge on the donor atom goes down correspondingly. It is the region in which the IRC is essentially the proton motion and the OCO antisymmetric stretch (Fig.3.2, and 4.3). As noted earlier, in chapter 3 (Fig. 3.7) the proton leaves its electronic charge behind, while it moves from the donor to the acceptor in the middle region of IRC. This increases the electronic charge on the donor. At the same time the acceptor charge increases steeply. The electrons in the n_σ orbital on the acceptor delocalize into the now vacant hydrogen atomic orbital forming the new hydrogen-acceptor bond. This hastens the process of the OCO rearrangement. This process is complete by the time the system reaches the point at IRC = +0.5.

We next turn to the IRC of the malonaldehyde. The charges on the donor and acceptor atoms of the malonaldehyde are presented in Fig. 4.6. Unlike the FAD case, the charge on the donor decreases to a noticeable extent (From $-0.49e$ to $-$

0.51e) in malonadehyde. At the same time the acceptor charge increases from –0.64e to –0.58e similar to the variations in FAD. This increased charge on the acceptor atom leads to the localization of the $\pi^*($ C=O) orbital on the carbon atom. Unlike in FAD there is no n_π orbital on the adjacent atom to provide electrons to the π^* orbital of the C=O. Instead, the electrons must come from the π-orbital between the two carbons located in the and β positions from the acceptor oxygen atom. This data is displayed in Fig. 4.7. Though the two sets of data do not match identically, they are nearly parallel. This indicates that, as the system moves along the IRC, the electrons from C=C π orbital move into the π^* orbital of the C=O bond. The associated stabilization energy is shown in Fig. 4.7b. As can be seen from the figure the amount of charge delocalization and the stabilization energy increase very little in the promoter mode controlled region of the IRC (<–0.2). Effectively, this delocalization of electrons that leads to the breaking of the C=O π-bond and formation of the new C=C contributes little to the energetics of the barrier. The last part of the puzzle in the formation of the double bond between the donor oxygen atom and the carbon atom adjacent to it. As the electrons flow out of the π-C=C bond through the β-carbon atom (with respect to acceptor oxygen) the co-efficient of the atomic orbital centered on the

69
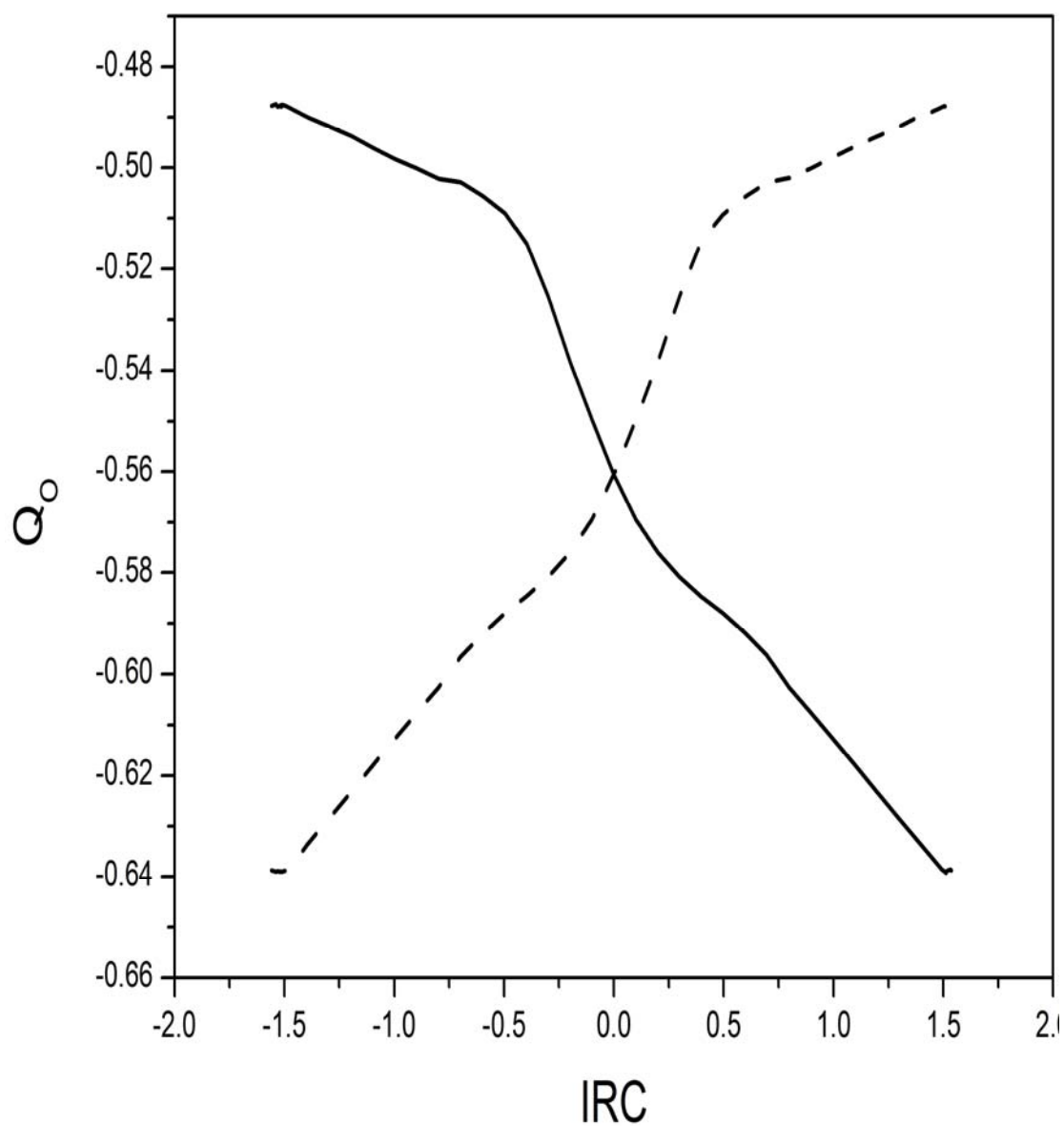
Fig. 4.6: Charges on the donor (——) and acceptor ((– – –) oxygen atoms in malonadehyde.

Fig. 4.7: a) The variation of population in π^* (C_2=O_1) (——) and the loss of population in the π (C_3=C_4) (– – –) orbital as a function of IRC in malonaldehyde. **b)** The Interaction energy of the π^* (C_2=O_1) and π (C_3=C_4) orbital in malonaldehyde.
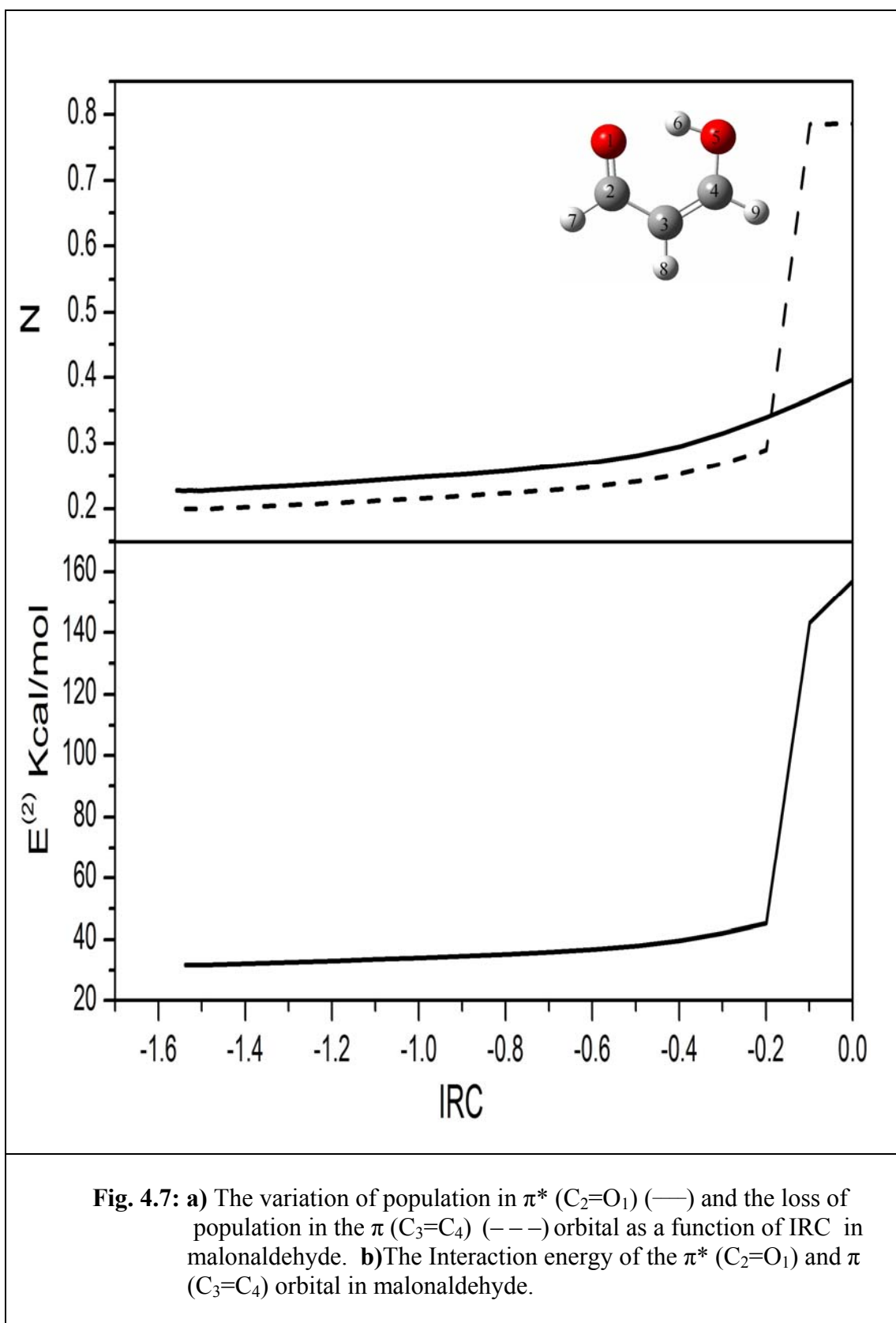
α-carbon atom increases in magnitude (Fig. 4.8). As a consequence its overlap with the n_π-orbital of the acceptor atom increases facilitating the donation of the electrons from the oxygen to the π^* orbital between the α and β carbon atoms. This data along with the stabilization energy this invokes is presented in Fig. 4.9. As can be seen, the variation of the population in π^*-orbital and the loss of population in n_π-orbital are consistent with each other. All the population transfer data and second order stabilization values show similar characterstics, a monotonic increase with a small slope upto about IRC $= -0.5$ and a sharp increase in the slope beyond that point reflecting the charge in the nature of the IRC at that point. This implies both the process ($\pi(C=C) \rightarrow \pi^*(C=O)$, $n_\pi(O_4) \rightarrow \pi^*(C=C)$) occur more are less simultaneously along with the proton migration after the promoter mode motion ceases. Once these process are over the molecule retreats along the promoter mode to its new equilibrium position.
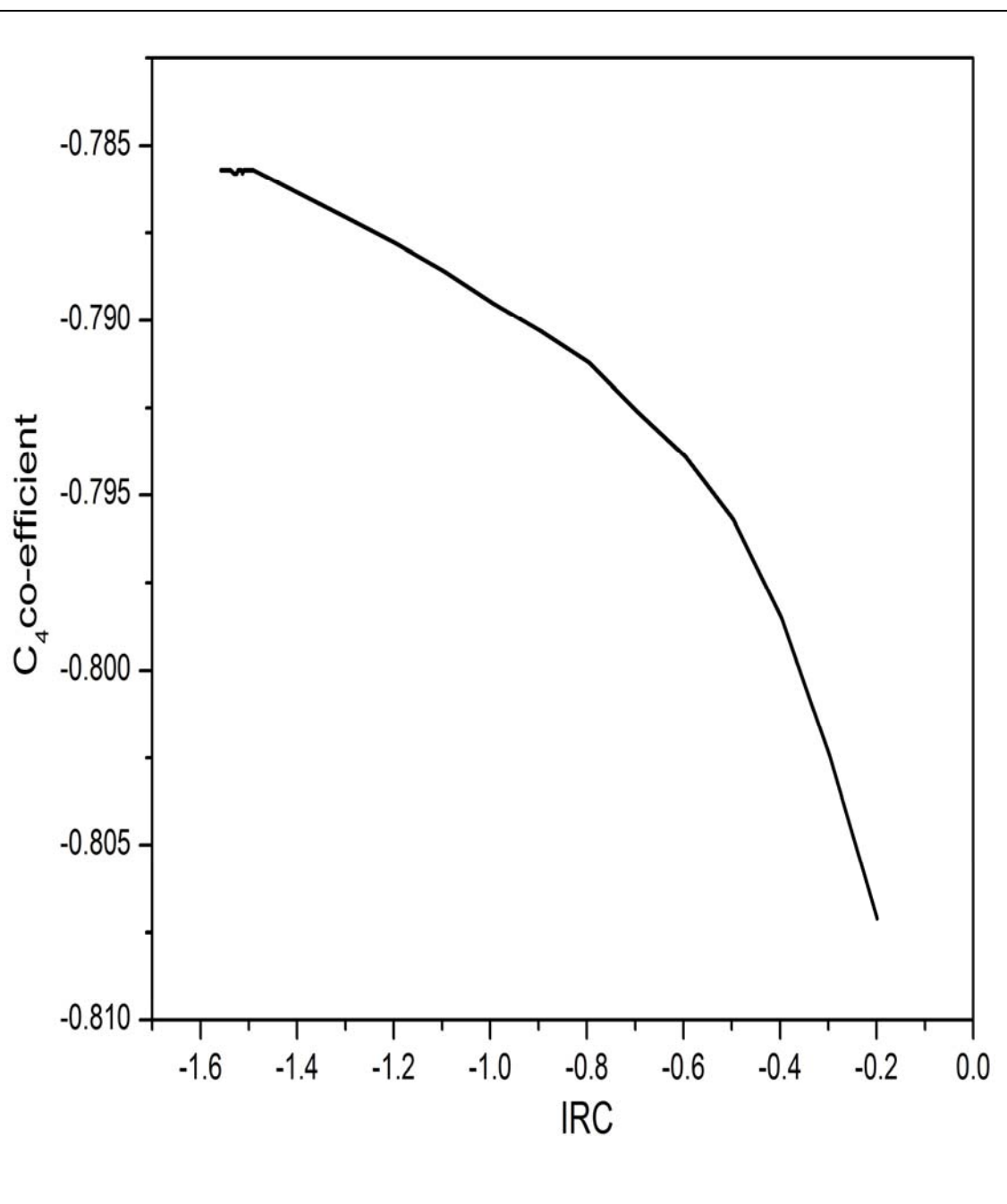
Fig. 4.8: The increase in magnitude of α-carbon (C_4) co-efficient of the atomic orbital along the IRC of malonaldehyde.

Fig. 4.9: a) The variation of population in π^* (C_3=C_4) (—) and the loss of population in the n_π ($- - -$) orbital of the donor oxygen atom as a function of IRC in malonaldehyde. **b)** The interaction energy of the π^*(C_3=C_4) and n_π (proton donor Oxygen lone pair) orbital in malonaldehyde.
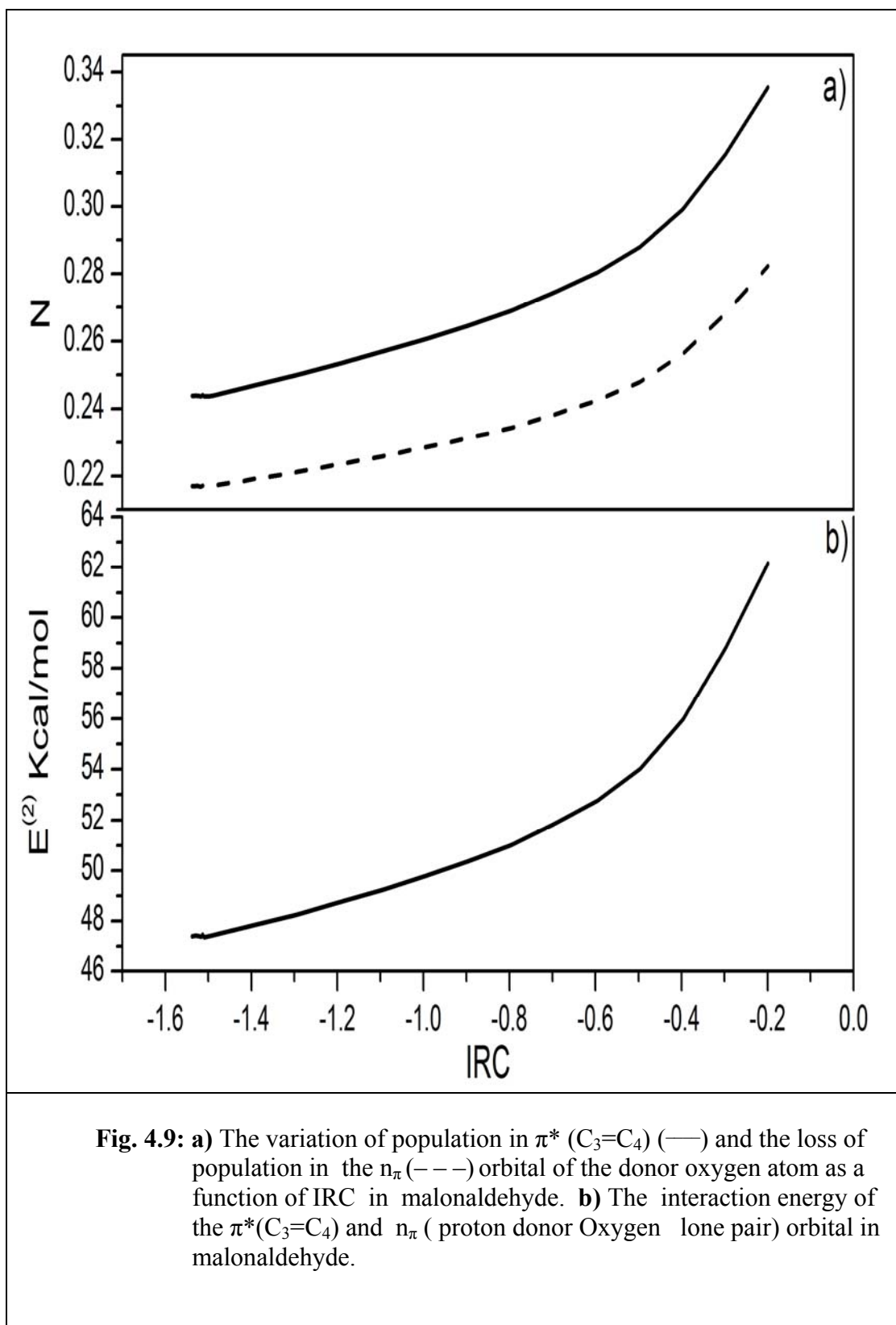
4.4   CONCLUDING REMARKS

We analyzed the nature of the electron flow among the π-orbitals in two model systems to understand the nature of the π-network reorganization. The vibrational modes associated with reorganization undergo a net displacement during the course of the reaction. Consequently, these must be classified as demoter modes accordingly to the Cui–Karplus criteria[1]. Interestingly, the major part of the movement along these co-ordinates is concurrent with the proton migration, i.e in the middle region of the IRC. They go through little change in the promoter mode dominated part of the IRC. The trigger for the motions are the changes in the charge on the acceptor atom. Since, the acceptor donates its n_σ electrons into the σ^* orbital of the hydrogen-donor bond, it becomes more   electrophilic in the first part of the IRC, where the promoter mode motion is the dominating feature. This increase in the electronegativity of the donor atom pulls the π-electron cloud towards it. This pulling is felt all the way up to the n_π electrons on the donor atom. It appears from the data we presented above, that the π electron reorganization goes through in one shot rather than a sequence of discrete steps.

REFERENCES

1. Cui, Q.; Karplus, M. *J. Phys. Chem. B* **2002**, *106*, 7927.

CHAPTER 5

MULTIPLE PROTON TRANSFER AND

KINETIC ISOTOPE EFFECT

5.1 INTRODUCTION

Kinetic isotope effect (KIE) is the dependence of the rate constant on the mass of the isotope of the atom in a chemical reaction. The primary kinetic isotope effect is the KIE when the bonds connecting that atom to the rest of the molecular frame are broken and reformed. If the isotope substitution is made away from the reaction center, the resulting KIE is called the secondary kinetic isotope effect. In both cases, the KIE arises from the increase in the activation energy when a lighter isotope is replaced by a heavier isotope. This is primarily due to the changes in the zero point energies in the reactant and the transition state due to isotope substitution.

Consider the primary KIE in a reaction involving the breaking of an X-H bond the reaction co-ordinate corresponds to the stretching mode of the X-H bond. At the transition state the frequency associated with the stretching motion becomes imaginary. From the transition state theory perspective the rate constant of this reaction is given by

$$k = \frac{k_B T}{h} . \exp\left[-(E_{el} - \frac{h\nu}{2}) / k_B T \right].$$
(5.1)

here, E_{el} is the electronic energy difference between the reactant and transition state structures, ν is the vibrational frequency of the X-H stretching mode in the reactant configuration, k_B is the Boltzman constant and the T is the temperature at which rate constant is measured. Implicit in this equation is the assumption that the ν is sufficiently large so that the associated partition functions can be taken as unity. When hydrogen atom is replaced by deuterium, ν decreases by almost a factor of $\sqrt{2}$. Consequently, the ratio of the two rate constant can be written as

$$\frac{k_H}{k_D} \alpha \ e^{-\frac{h(\nu_H - \nu_D)}{2 k_B T}}$$
(5.2)

More generally, in a polyatomic system one can write

$$\frac{k_H}{k_D} \alpha \ e^{-\frac{(\Delta ZPE_H - \Delta ZPE_D)}{k_B T}}$$
(5.3)

here, ΔZPE is the difference between the zero point energies at the transition state and the reactant

$$\Delta ZPE = ZPE^{\neq} - ZPE^{R}$$
(5.4)

For a typical X-H bond, the X-H stretch frequency is about 3000 cm^{-1}. From this, it follows that the k_H/k_D is about 7 at room temperature. Deviations from this number are indicative of the influence of other mechanisms. In particular quantum mechanical tunneling has been invoked by several authors to explain such deviations[1-4]. Several indices have been proposed to estimate the influence of tunneling. These include the Swain-Schaad exponential relation[5,6] and related approaches.

We have seen in chapter 1 that the role of the promoter mode is to enhance the delocalization of the n_σ electrons of the acceptor atom in to the $\sigma*$ orbital of the donor hydrogen covalent bond. One of the consequences of this is that the donor-hydrogen stretch frequency goes down and ultimately becomes imaginary in the neighborhood of the transition state. In the case of concerted multiple proton transfer reactions, not only does the reaction co-ordinate frequency become imaginary, the other hydrogen stretch frequencies also come down because of the reduced bond strengths of donor-hydrogen bonds. In the case of (HF)$_3$, FAD this decrease is about $1300 - 1500$ cm^{-1}. The hydrogen bend frequencies, on the other hand, increase slightly, by about 300–400 cm^{-1}. Consequently, the overall zero point energy comes down as one moves to the transition state from the reactant. In addition it appears as if the fall in the zero point energy is almost linearly proportional to the number of protons that migrate in a concerted manner. This is because there would be n-lone pairs located on n acceptor atom that delocalize into corresponding n $\sigma*$ orbitals, lowering bond

strength of n covalent bonds that hold hydrogen atoms with the donor atoms. While one of the hydrogen stretch modes becomes reaction co-ordinate, the remaining n-1 vibrations go down leading to the drop in the zero point energy proportional to n. If so, the KIE (k_H/k_D) should vary exponentionally with the number of deuterium atoms that are substituted.

The goal of the present chapter is to test the this hypothesis computationally. We study three systems, FAD, $(HF)_3$ and $(H_2O)_n$. We substitute the hydrogens with deuterium sequentially and calculate the changes in ΔZPE as the number of deuterium atoms in the system increases. In the case of FAD it is possible to substitute the hydrogen attached to the carbon atom. According to our analysis of chapter 3 this should have minimal effect on ΔZPE since, the C-H bond remains practically a spectator to the proton transfer reaction. We verify this. The water clusters provide a class of systems in which the number of protons that undnergo cyclic exchange can be systematically increased. We verify that the ΔZPE in these systems increases nearly linearly with the number of protons that are exchanged.

5.2 RESULTS AND DISCUSSIONS

We have taken the reaction and transition state structures of FAD and $(HF)_3$ and carried out a frequency calculation after replacing the hydrogen with deuterium. The resulting frequencies were used to calculate the various $\Delta ZPE`s$. In the case of water clusters, there have been several works in recent past to

determinine their structure and other equilibrium properties[7-15]. We have taken the geometric parameters from Ref. 7 as the starting point and optimized the structure once again with B3LYP/aug-cc-pVTZ level of theory for n = 3–6 clusters. The transition states were obtained by the usual procedure implemented in Gausssian suite of programs. Frequencies were obtained at the optimized geometries. The most stable structures for n = 3–5 clusters are cyclic-clusters. The most stable cluster for n = 6 structure is a cage structure[7]. Since this will not support a concerted 6 proton transfer, we choose to study the chair form of a cyclic structure analyzed by Xanthia`s and Dunning[8]. This structure supports a concerted six proton transfer. The optimized structural parameters and the vibrational frequencies of these molecules are presented in the Appendix. We now consider the effect of deuterium substitution on ΔZPE for the individual molecular systems.

5.2.1 (HF)$_3$

Four isotopomers of (HF)$_3$ are analyzed, (HF)$_3$, (HF)$_2$(DF), (HF)(DF)$_2$ and (DF)$_3$. The variation of the ΔZPE among these four isotopomers is presented in Table 5.1. As can be seen from this data the *ΔZPE* increases almost linearly with each additional deuterium atom. The over all threshold energy for the reaction is given by

$$E_{th} = E_{el} + \Delta ZPE \tag{5.5}$$

Since, E_{el} is independent of the isotope, E_{th} depends essentially on the ΔZPE. We present in Fig. 5.1, the variation of E_{th} as a function of the number of deuterium atoms. As can be seen the threshold energy increased almost linearly with the number of deuterium atoms.

TABLE. 5.1: The zero point barrier of $(HF)_3$ and the each hydrogen replaced by deuterium.

S. No	MOLECULE	$\Delta ZPE = (ZPE_{TS})^{\neq}-(ZPE^{R})$ (kcal/mol)
1	$(HF)_3$	-2.97
2	$(HF)_2(DF)$	-2.61
3	$(HF)(DF)_2$	-2.22
4	$(DF)_3$	-1.81
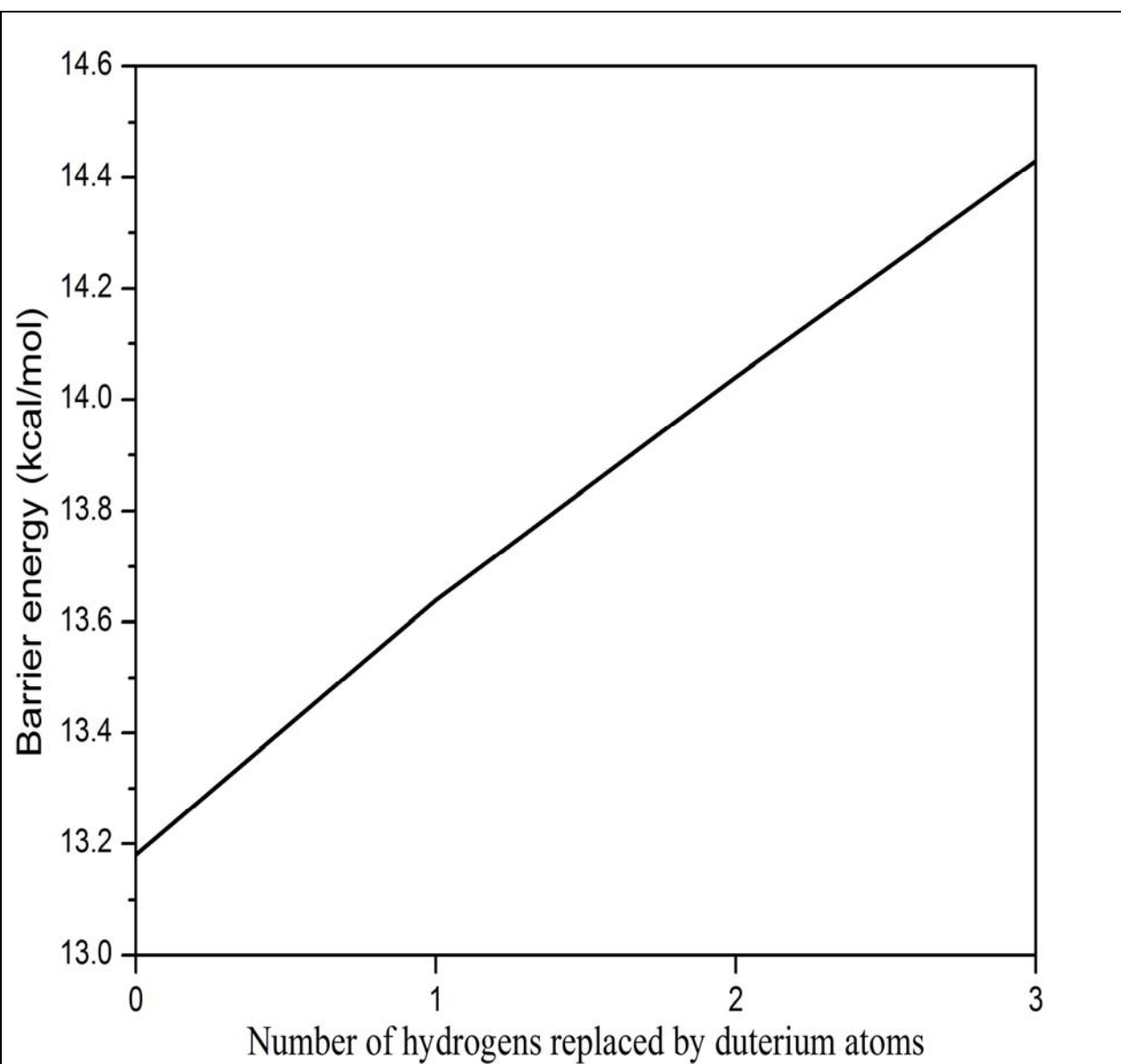
Fig. 5.1: Threshold energy to proton transfer in (HF)$_3$ with sequential deuterium Substitution.

5.2.2 FAD

There are two groups of hydrogens in FAD, those that are attached to the oxygen atoms and undergo reaction and those that are attached to the carbons and remains spectators to the proton exchange. We have calculated the variation of *ΔZPE* in four of the isotopomers of FAD. These results are collected in Table. 5.2. The *ΔZPE* of $(HCOOH)_2$ and $(DCOOH)_2$ are practically identical implying that the secondary KIE in this case is negligible. This is to be expected since, the C-H vibrational frequencies change little along the IRC as we saw in chapter 3. Replacing the O-H protons increases *ΔZPE* almost linearly with about 0.68 kcal/mol contribution for each hydrogen replacement. This number is to be contrasted with an increase of about 0.39 kcal/mol in the case of $(HF)_3$.

Table. 5.2: The zero point barrier of FAD and the each hydrogen replaced by deuterium.

S. No	MOLECULE	$\Delta ZPE = (ZPE^{\neq}) - (ZPE^{R})$ kcal/mol
1	FAD	–4.04
2	(HCOOD)(HCOOH)	–3.38
3	$(HCOOD)_2$	–2.69
4	$(DCOOH)_2$	–4.05

5.2.3 (H₂O)ₙ

Isotopomers of four water clusters were studied. Three classes of isotopomers were considered. All hydrogen systems, clusters with hydrogen bond forming hydrogens replaced by deuterium and finally, clusters in which all the hydrogen atoms replaced by deuterium. The results are presented in Table. 5.3. Since we have considered only cyclic clusters, each n cluster under goes a concerted n proton transfer. From the data of Table 5.3 it is apparent that ΔZPE decreases almost linearly with the number of protons that migrate to the other side of the hydrogen bond. For example, in the all hydrogen clusters the ΔZPE decreases by about 2.3 kcal/mol for each molecule of water added to the cluster with a maximum deviation of about 0.26 kcal/mol. Similar trends hold for other two isotopomers also.

Table.5.3: The zero point barrier of (H₂O)ₙ and the each hydrogen replaced by deuterium.

S. No	Number of water clusters	ΔZPE with all hydrogens(kcal/mol)	ΔZPE with innerdueterium (kcal/mol)	ΔZPE with all duterium (kcal/mol)
1	$(H_2O)_3$	−3.99	−2.33	−2.53
2	$H_2O)_4$	−6.16	−3.76	−3.97
3	$(H_2O)_5$	−8.28	−5.22	−5.41
4	$(H_2O)_6$	−10.92	−7.01	−7.22

Comparing the two classes of isotopomers, the all deuterium one and the one in which the inner hydrogens (that are part of the hydrogen bond), we note that *ΔZPE* values are practically identical. They differ by about 0.2 kcal/mol in all the four clusters. This small difference must be due to second order KIE.

5.3 CONCLUDING REMARKS

In this chapter we have analyzed the variation of *ΔZPE* on the number of protons that undergo a concerted transfer. Each of these n D-H covalent bonds receive donations from the lone pairs on the associated acceptor atoms as a consequence of promoter mode motion. Out of the n D-H stretch modes one turns imaginary at the transition state. This mode represents the concerted n-proton transfer reaction co-ordinate. However, all the force constants associated with the D-H stretch modes go down more are less uniformly depending on the nature of the donor and acceptor atoms and the hydrogen bond between them. Consequently, the frequencies of all the *normal modes* associated with D-H stretch motion decreases as one travels along the IRC. Note that the net charge transfer from the acceptor n_σ lone pairs of the acceptor atom to the σ* (D-H) orbitals increases linearly with n to the leading order. As a result of drastic fall in the stretch vibrational frequencies the overall zero point energy decreases significantly at the transition state. Since, this decrease in the transition state zero point energy is proportional to n the *ΔZPE* also falls (approximately linearly) as n increases.

Since the *ΔZPE* effects the rate constant in an exponential manner, the KIE measured as k_H/k_D also depends on the number of protons being exchanged exponentially. Such exponential dependence was noted by earlier authors[16,17]. Venkatsubban and Silverman[16] measured the CO_2 hydration catalyzed by carbonic anhydrase enzyme in mixture of water and deuterium oxide. The rate constant for this reaction was calculated by Smedarchina *et al*[17]. Both of them noted that the KIE`s have an exponential dependence on the deuterium concentration in the H_2O/D_2O mixture and concluded that the reaction undergoes a concerted transfer through a bridge of two water molecules. Indeed Smedrachina and co-workers[17] noted that the large KIE is due to the accumulation of zero point energy differences. Obviously, this decrease in zero point energy is due to the donation of acceptor atom lone pair in to the σ* (D-H) orbitals.

REFERENCES

(1) Doering, W. E.; Zhao, X. *J. Am. Chem. Soc.* **2006**, *128*, 9080.

(2) Pang, J.; Hay, S.; Scrutton, N.S.; Sutcliffe, M. J. *J. Am. Chem. Soc.* **2008**, *130*, 7092.

(3) Nagel, Z, D.; Kilman J. P. *Chem. Rev.* **2006**, *106*, 3095.

(4) Knapp, M. J.; Rickert, K.; Kilman, J. P. *J. Am. Chem. Soc*. **2002**, *124*, 3865.

(5) Swain, C. G.; Stivers, E. C.; Reuwer, J. F, Shaad, L. J. *J. Am. Chem. Soc.* **1958**, *80*, 5885

(6) Kohen, A.; Jensen, J. H. *J. Am. Chem. Soc.* **2002**, *124*, 3858.

(7) Maheshwary, S.; Patel, N.; Satyamurthy, N. *J. Phys. Chem. A* **2001**, *105*, 10525.

(8) Xantheas, S.S.; Dunning, Jr. T. H *J. Chem. Phys.* **1993**, *99*, 8774.

(9) Loerting, T.; Liedl, K. R.; Rode, B. R. *J. Chem. Phys.* **1998**, *109*, 2672.

(10) Kang, D.; Dai, J.; Hou, Y.; Yuan, J. *J. Chem. Phys.* **2010,** *133*, 014302.

(11) Mandziuk, M. *J. Phys. Chem. A.* **2004,** *108*, 121.

(12) Znamenskiy, V. S.; Green, M. E.; *J. Chem. Theory Comput.* **2007**,*3*, 103.

(13) Liu, K.; Brown, M. G.; Cruzan, J. D.; Saykally, R. J. *J. Phys. Chem. A* **1997**, *101*, 9011.

(14) Liu, K.; Brown, M. G.; Carter, C.; Saykally, R. J.; Gregory, J. K.; Clary, D. C. *Nature*, **1996**, *381*, 501.

(15) Liu, K.; Cruzan, J. D.; Saykally, R. J. *Science*, **1996**, *271*, 929.

(16) Smedarchina, Z.; Siebrand, W.; Fernandez-Ramos, and Cui, Q *J. Am. Chem. Soc.* **2003**, *125*, 243.

(17) Venkatasubban, K.S.; Silverman, D.N. *Biochemistry* **1980**, *19*, 4984.

CHAPTER 6

CONCLUDING REMARKS

Our goal in this thesis was the exploration of the electronic origin of promoter modes that are symmetrically coupled to the reaction co-ordinate in proton transfer reactions. In a proton exchanging hydrogen bonded complexes, the acceptor atom has a lone pair oriented towards the hydrogen atom bound to the donor moiety. We suggested that, as the complex moves along the promoter mode, the acceptor atom donates its lone pair in to the antibonding orbital of the sigma bond between the hydrogen and the donor atom. As a consequence of such delocalization, the bond between these two atoms is weakened to a significantly greater extent than at the reactant equilibrium geometry, and the proton transfer goes through a smaller barrier.

To test the above hypothesis we studied a few proto-typical hydrogen transfer reaction systems, cyclic $(HF)_3$, formic acid dimer, malonaldehyde and some

water clusters. We found that the acceptor lone pairs do indeed delocalize into the σ* orbitals of the covalet bond connecting the donor and hydrogen atoms. Thus, from an electronic structure perspective a promoter mode can be defined as the vibrational mode that promotes the delocalization of the acceptor lone pair of electrons in to the σ* orbital of the DH covalent bond by bringing about a greater overlap between the σ*(DH) and n_σ (A) orbitals. In all the above systems, from the electronic structure calculations (IRC,NBO, Mulliken charge analysis) carried by us, it is evident that, the donor-acceptor stretch mode is symmetrically coupled to the proton transfer co-ordinate. The motion along the promoter seems to be, both before and after the proton migration but rarely concurrent with it.

From the Studies presented in the chapter 3 on $(HF)_3$ and FAD it is evident that, about 0.2e are donated in to the DH(σ*). The second order interaction energy of the lone pair orbital(n_σ) and HF(σ*) of $(HF)_3$ increased from 10 kcal/mol to 50 kcal/mol and that of FAD, the lone pair orbital (n_σ) and OH(σ*) orbital second order interaction energy increased from 10 kcal/mol to 60 kcal/mol. Because of this donation, the DH bond becomes weaker and its stretch frequency goes down, while the bend frequencies go up marginally. During the proton transfer charge on the transferring hydrogen changes. A mathematical model is developed for the change of charge on the transferring hydrogen atom during the proton transfer for FAD and $(HF)_3$ molecule.

During the proton transfer in π bonded systems, π bonds reorganize themselves to compensate the charge imbalance the donation of the n_σ lone pair

electrons into DH(σ*) orbital during the proton transfer. To this end we analyzed in chapter 4 FAD and malonaldehyde. In FAD there is no change in the charge of the donor atom in the promoter mode regime. The charge on the acceptor atom increases from –0.5e to –0.45e as the molecules moves from reactant to about IRC = –0.5. To compensate this loss of charge, the acceptor oxygen pulls the π electrons of the C=O towards itself. Consequently, π* (C=O) orbital becomes more localized on the carbon atom. This increases the overlap between the n_π(donor) orbital and the π*(C=O) orbital. The second order interaction energy of donor n_π orbital and π*(C=O) orbital increases from 65 kcal/mol to ~100 kcal/mol. In case of malonaldehyde the charge on the acceptor increases from -0.64e to -0.58e.   This increased charge on the acceptor atom leads to the localization of the π*(C=O) orbital on the carbon atom. Unlike in FAD there is no n_π orbital on the adjacent atom to provide electrons to the π* orbital of the C=O. Instead, the electrons must come from the π-orbital between the two carbons located in the and β positions from the acceptor oxygen atom. There are two π bonds in this system and the one n_π on donor atom undergoes loss of electrons. Their population transfers and second order interaction energies are presented.

Finally, we have studied the effect of isotope substitution on the barrier energy on water clusters and (HF)$_3$ and FAD in chapter 5. We have seen that the fall in zero point energy is almost proportional to the number of protons that are transferred in a concerted manner. This is because there are n lone pairs that are

located on n acceptor atom that delocalize into corresponding n σ* orbitals lowering bond strength of n covalent bonds that hold the hydrogen atoms with the donor atoms. The D-H stretch modes goes down by about 1300-1500 cm^{-1} and the bend modes goes up by about 300-400 cm^{-1}.

APPENDIX

Table A-1a): Reactant geometry of (HF)$_3$

Symbolic Z-matrix

Charge = 0 Multiplicity = 1

```
F
F         1   B1
F         2   B2    1   A1
H         1   B3    3   A2    2   D1
H         2   B4    4   A3    1   D2
H         3   B5    5   A4    2   D3
```

B1=2.58607144
B2=2.58607144
B3=0.94694358
B4=0.94694358
B5=0.94694358
A1=60.
A2=81.1147584
A3=92.4435606
A4=92.4435606
D1=0.
D2=0.
D3=0.
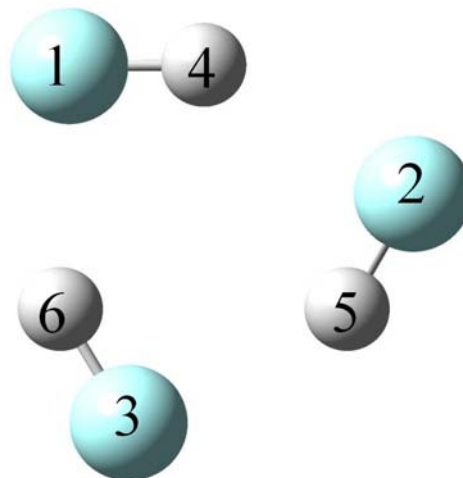
Table A-1b): Transition state geometry of (HF)$_3$

Symbolic Z-matrix

Charge = 0 Multiplicity = 1

```
F
F          1   B1
F          2   B2    1   A1
H          1   B3    3   A2    2   D1
H          2   B4    4   A3    1   D2
H          3   B5    5   A4    2   D3
```

B1=2.25918934
B2=2.25918934
B3=1.16288796
B4=1.16288796
B5=1.16288796
A1=60.
A2=73.743226
A3=87.48645201
A4=87.48645201
D1=0.
D2=0.
D3=0.
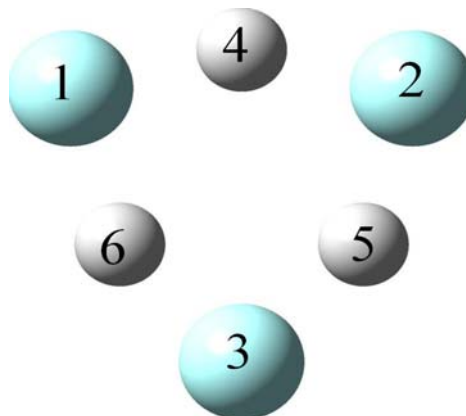
Table A-2: Reactant and transition state vibrational frequencies of $(HF)_3$

S.NO	Reactant (cm^{-1})	Transition state (cm^{-1})
1	209	1645 i
2	209	548
3	228	548
4	530	711
5	530	1017
6	651	1017
7	651	1280
8	726	1510
9	1025	1510
10	3573	1743
11	3711	1743
12	3711	2045

Table A-3a: Reactant geometry of FAD

Symbolic Z-matrix

Charge = 0 Multiplicity = 1

C							
O	1	B1					
O	1	B2	2	A1			
H	3	B3	1	A2	2	D1
H	1	B4	3	A3	4	D2
C	1	B5	3	A4	4	D3
O	6	B6	1	A5	3	D4
O	6	B7	1	A6	3	D5
H	8	B8	6	A7	7	D6
H	6	B9	8	A8	9	D7

B1=1.21843483
B2=1.30992146
B3=1.00239621
B4=1.09476384
B5=3.79734195
B6=1.21843483
B7=1.30992146
B8=1.00239621
B9=1.09476384
A1=126.3227891
A2=110.88422412
A3=111.8566565
A4=66.74709127
A5=59.57569783
A6=66.74709127
A7=110.88422412
A8=111.8566565
D1=0.
D2=180.
D3=0.
D4=0.
D5=180.
D6=0.
D7=180.

Table A-3b): Transition state geometry of FAD

Symbolic Z-matrix

Charge = 0 Multiplicity = 1

```
C
O        1   B1
O        1   B2     2   A1
H        3   B3     1   A2     2   D1
H        1   B4     3   A3     4   D2
C        1   B5     3   A4     4   D3
O        6   B6     1   A5     3   D4
O        6   B7     1   A6     3   D5
H        8   B8     6   A7     7   D6
H        6   B9     8   A8     9   D7
```

B1=1.25963823
B2=1.25963823
B3=1.21005132
B4=1.09404496
B5=3.55071962
B6=1.25963823
B7=1.25963823
B8=1.21005132
B9=1.09404496
A1=126.65580793
A2=115.8558688
A3=116.67209603
A4=63.32790397
A5=63.32790397
A6=63.32790397
A7=115.8558688
A8=116.67209603
D1=0.
D2=180.
D3=0.
D4=0.
D5=180.
D6=0.
D7=180.
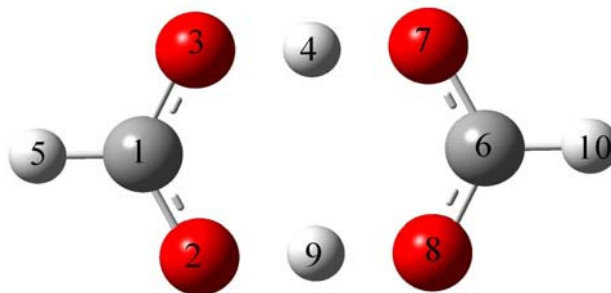
Table A-4: Vibrational frequencies of FAD

S.NO	Reactant (cm^{-1})	Transition state (cm^{-1})
1	78	1234 i
2	175	87
3	187	231
4	212	232
5	261	300
6	281	508
7	690	573
8	723	748
9	983	800
10	1002	1071
11	1079	1077
12	1102	1262
13	1257	1308
14	1260	1353
15	1402	1398
16	1404	1398
17	1449	1401
18	1481	1403
19	1693	1564
20	1767	1666
21	3039	1722
22	3055	1739
23	3066	3069
24	3160	3071

Table A-5a): Reactant geometry of malonaldehyde

Symbolic Z-matrix

Charge = 0 Multiplicity = 1

```
O
C          1   B1
C          2   B2    1   A1
C          3   B3    2   A2    1   D1
O          1   B4    2   A3    3   D2
H          5   B5    4   A4    3   D3
H          2   B6    3   A5    4   D4
H          3   B7    4   A6    5   D5
H          4   B8    5   A7    6   D6
```

B1=1.24506296
B2=1.43997513
B3=1.36807972
B4=2.60796935
B5=1.00210005
B6=1.10420094
B7=1.08423788
B8=1.08796844
A1=123.47445616
A2=120.00475008
A3=87.44446152
A4=106.76475308
A5=117.69860275
A6=119.85861206
A7=112.99901438
D1=0.
D2=0.
D3=0.
D4=180.
D5=180.
D6=180.
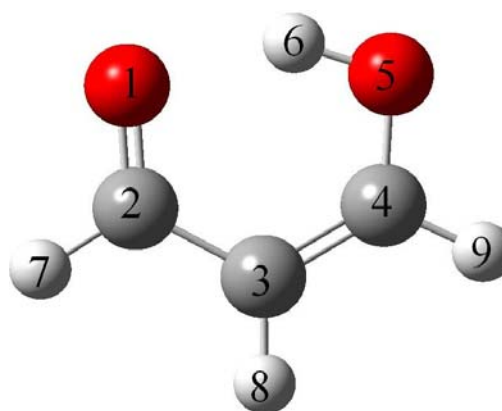
Table-5b) Transition state geometry of malonaldehyde

Symbolic Z-matrix

Charge = 0 Multiplicity = 1

```
O
C          1   B1
C          2   B2    1   A1
C          3   B3    2   A2    1   D1
O          1   B4    2   A3    3   D2
H          5   B5    4   A4    3   D3
H          2   B6    3   A5    4   D4
H          3   B7    4   A6    5   D5
H          4   B8    5   A7    6   D6
```

B1=1.27670066
B2=1.39522466
B3=1.39522466
B4=2.37010794
B5=1.21112009
B6=1.09108849
B7=1.077099
B8=1.09108849
A1=121.69813697
A2=116.48730493
A3=90.05821056
A4=101.96690764
A5=121.2700452
A6=121.75634753
A7=117.03181783
D1=0.
D2=0.
D3=0.
D4=180.
D5=180.
D6=180.
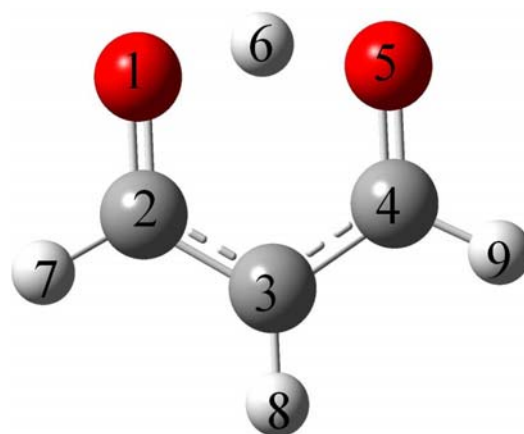
Table A-6: Reactant and transition state vibrational frequencies of
malonaldehyde

S.NO	Reactant (cm^{-1})	Transition state (cm^{-1})
1	282	1173 i
2	288	370
3	402	397
4	522	576
5	792	619
6	896	788
7	947	949
8	1003	1003
9	1026	1049
10	1050	1061
11	1117	1113
12	1288	1299
13	1390	1333
14	1406	1372
15	1480	1507
16	1626	1613
17	1694	1635
18	2969	1880
19	3094	3084
20	3173	3084
21	3217	3233

Table A-7a): Reactant geometry of $(H_2O)_3$

Symbolic Z-matrix

Charge = 0 Multiplicity = 1

```
O
H        1   B1
H        1   B2    2   A1
O        1   B3    3   A2    2   D1
H        4   B4    1   A3    3   D2
H        4   B5    1   A4    3   D3
O        4   B6    1   A5    6   D4
H        7   B7    1   A6    4   D5
H        7   B8    1   A7    4   D6
```

B1=0.9758946
B2=0.96097938
B3=2.79664188
B4=0.97521195
B5=0.96075596
B6=2.8053806
B7=0.97596839
B8=0.96069435
A1=106.29312605
A2=116.86828649
A3=80.1629235
A4=128.19218709
A5=59.90707846
A6=19.03554524
A7=118.21056624
D1=17.13620173
D2=122.70600446
D3=-134.01058987
D4=-107.76224878
D5=178.73187367
D6=-126.13544564

103

Table A-7b): Transition state geometry of $(H_2O)_3$

Symbolic Z-matrix

Charge = 0 Multiplicity = 1

O							
H	1	B1					
H	1	B2	2	A1			
O	1	B3	3	A2	2	D1
H	4	B4	1	A3	3	D2
H	4	B5	1	A4	3	D3
O	4	B6	1	A5	6	D4
H	7	B7	1	A6	4	D5
H	7	B8	1	A7	4	D6

B1=1.22146316
B2=0.96149854
B3=2.38276052
B4=1.22408142
B5=0.96107599
B6=2.38130884
B7=1.22217693
B8=0.96111334
A1=112.2244167
A2=117.07164201
A3=72.89673076
A4=117.36679764
A5=60.02068128
A6=12.82057679
A7=117.34450637
D1=13.08998372
D2=111.11896272
D3=-141.04718799
D4=-111.85384689
D5=177.98494075
D6=-111.78791271
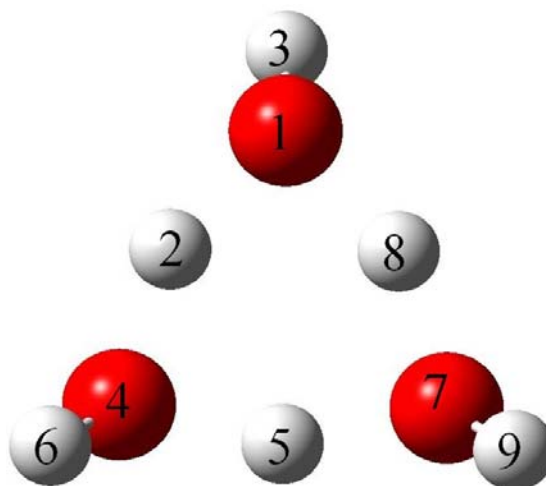
Table A-8: Reactant and transition state vibrational frequencies of $(H_2O)_3$

S.NO	Reactant (cm^{-1})	Transition state (cm^{-1})
1	175	1807 i
2	183	440
3	191	449
4	210	504
5	215	545
6	248	551
7	353	665
8	364	682
9	453	728
10	584	767
11	673	1178
12	873	1179
13	1635	1381
14	1638	1533
15	1659	1561
16	3530	1595
17	3592	1680
18	3602	2001
19	3864	3845
20	3868	3849
21	3869	3851

Table A-9a): Reactant geometry of $(H_2O)_4$

Symbolic Z-matrix

Charge = 0 Multiplicity = 1

O							
O	1	B1					
O	2	B2	1	A1			
O	3	B3	2	A2	1	D1	
H	1	B4	2	A3	3	D2	
H	1	B5	2	A4	3	D3	
H	2	B6	1	A5	4	D4	
H	3	B7	2	A6	1	D5	
H	4	B8	3	A7	2	D6	
H	4	B9	3	A8	2	D7	
H	3	B10	2	A9	1	D8	
H	2	B11	1	A10	4	D9	

B1=2.7402554
B2=2.74021781
B3=2.74024737
B4=0.98382922
B5=0.96093959
B6=0.96093726
B7=0.98383252
B8=0.98383296
B9=0.96093827
B10=0.96093881
B11=0.98383448
A1=89.99772992
A2=89.99499321
A3=8.04959245
A4=110.03276303
A5=122.10016296
A6=97.98343412
A7=97.98649986
A8=122.06143413
A9=122.03820014
A10=97.99505354
D1=-0.9623086
D2=-171.6283204
D3=125.34502877
D4=114.89856899
D5=0.05109966
D6=-0.05510913
D7=114.84194002
D8=-114.83257585
D9=-0.02670112
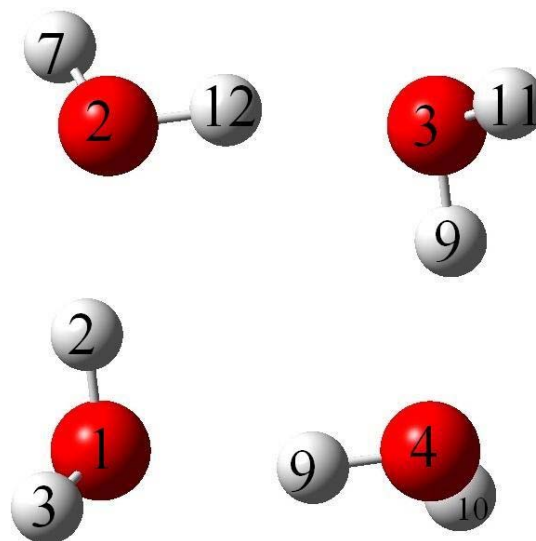
Table A-9b): Transition state geometry of $(H_2O)_4$
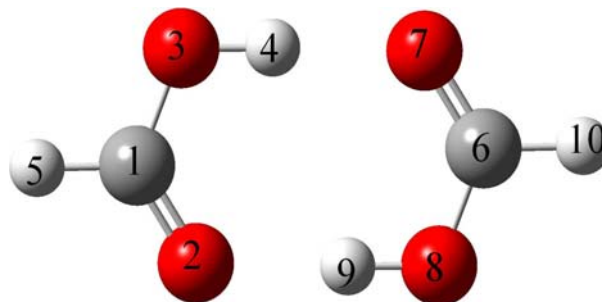
Symbolic Z-matrix

Charge = 0 Multiplicity = 1

```
O
O              1    B1
O              2    B2     1    A1
O              3    B3     2    A2     1    D1
H              1    B4     2    A3     3    D2
H              1    B5     2    A4     3    D3
H              2    B6     1    A5     4    D4
H              3    B7     2    A6     1    D5
H              4    B8     3    A7     2    D6
H              4    B9     3    A8     2    D7
H              3    B10    2    A9     1    D8
H              2    B11    1    A10    4    D9
```

B1=2.41103993
B2=2.41103992
B3=2.41104061
B4=1.21136378
B5=0.96108256
B6=0.96108257
B7=1.2113696
B8=1.21136194
B9=0.96108268
B10=0.96108255
B11=1.21136602
A1=89.92862559
A2=89.92878032
A3=5.62809083
A4=114.1746601
A5=114.1721988
A6=95.5532158
A7=95.55305041
A8=114.17163122
A9=114.17229374
A10=95.55311868
D1=-4.04086856
D2=-177.99685373
D3=120.67477871
D4=120.67664509
D5=-4.24164517
D6=4.24152642
D7=120.67590252
D8=-120.67701222
D9=4.24156118

107
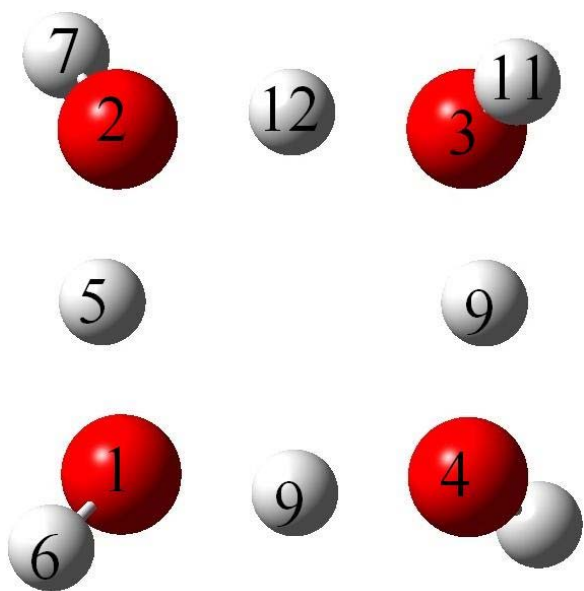
Table A-10: Reactant and transition state vibrational frequencies of $(H_2O)_4$

S.NO	Reactant (cm^{-1})	Transition state (cm^{-1})
1	53	1645 i
2	88	86
3	207	153
4	221	396
5	242	427
6	242	427
7	259	561
8	259	584
9	259	589
10	301	611
11	415	621
12	450	621
13	463	681
14	463	681
15	765	740
16	832	1060
17	832	1060
18	992	1389
19	1641	1470
20	1655	1514
21	1655	1514
22	1685	1558
23	3332	1598
24	3430	1612
25	3430	1612
26	3470	1814
27	3860	3849
28	3861	3849
29	3861	3849
30	3862	3850

Table A-11a): Transition state geometry of $(H_2O)_5$

Symbolic Z-matrix

Charge = 0 Multiplicity = 1

O						
H	1	B1				
H	1	B2	2	A1		
O	1	B3	3	A2	2	D1
H	4	B4	1	A3	3	D2
H	4	B5	1	A4	3	D3
O	4	B6	1	A5	3	D4
H	7	B7	4	A6	1	D5
H	7	B8	4	A7	1	D6
O	7	B9	4	A8	1	D7
H	10	B10	7	A9	4	D8
H	10	B11	7	A10	4	D9
O	10	B12	7	A11	4	D10
H	13	B13	10	A12	7	D11
H	13	B14	10	A13	7	D12

B1	0.97645400
B2	0.96082888
B3	2.68466344
B4	0.98448850
B5	0.96061356
B6	2.73102686
B7	0.98294200
B8	0.96047965
B9	2.71438145
B10	0.98480898
B11	0.96089467
B12	2.71729730
B13	0.98187904
B14	0.96070824
A1	99.62349444
A2	99.63106816
A3	111.08173102
A4	111.74490402
A5	107.33654835
A6	108.39041072
A7	116.56113339
A8	108.38981499
A9	108.72416886
A10	114.75623420
A11	107.67995160
A12	107.57020936
A13	114.59632162
D1	0.00479388
D2	-125.62237345
D3	115.97584405
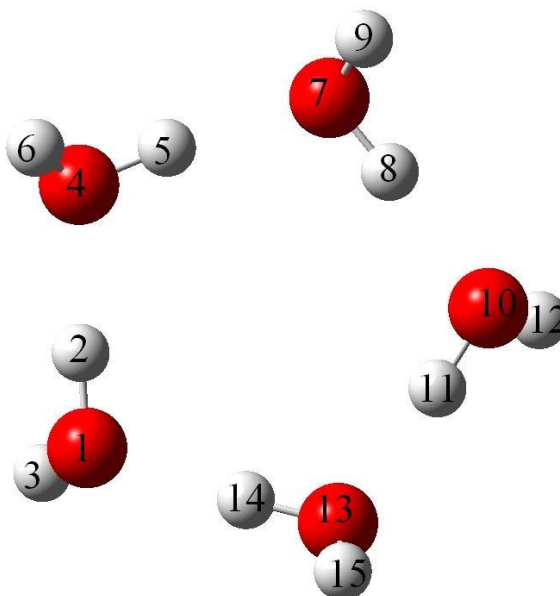
D4   -121.82839950
D5   0.00000000
D6   -125.80644565
D7   0.00340148
D8   -1.09575723
D9   116.65353605
D10   -0.00000000
D11   -0.00647849
D12   -114.07869425

Table-11b): Transition state geometry of $(H_2O)_5$
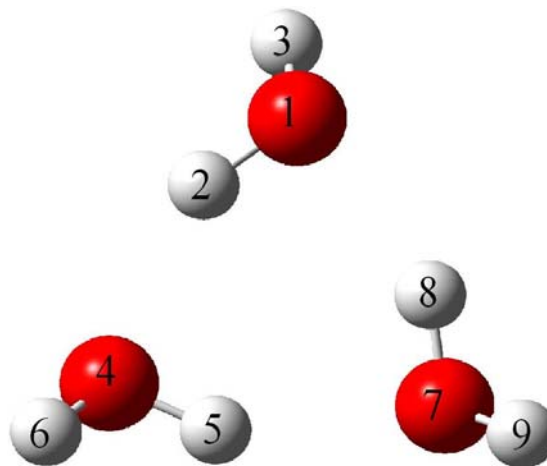Symbolic Z-matrix
Charge = 0 Multiplicity = 1

```
O
H              1    B1
H              1    B2     2    A1
O              1    B3     3    A2     2    D1
H              4    B4     1    A3     3    D2
H              4    B5     1    A4     3    D3
O              4    B6     1    A5     3    D4
H              7    B7     4    A6     1    D5
H              7    B8     4    A7     1    D6
O              7    B9     4    A8     1    D7
H             10    B10    7    A9     4    D8
H             10    B11    7    A10    4    D9
O             10    B12    7    A11    4    D10
H             13    B13   10    A12    7    D11
H             13    B14   10    A13    7    D12
```

B1=1.20278405
B2=0.96101032
B3=2.41282377
B4=1.2086057
B5=0.96051595
B6=2.41427008
B7=1.21088967
B8=0.96051913
B9=2.41264978
B10=1.2081849
B11=0.96101314
B12=2.41229086
B13=1.20555421
B14=0.96085274
A1=110.20870151
A2=111.01413984
A3=110.26399355
A4=111.47833582
A5=107.94965488
A6=109.54571212
A7=114.58247764
A8=107.92804045
A9=109.749449
A10=111.01453486
A11=108.03534279
A12=109.61257068
A13=111.61948521
D1=-1.50825451
D2=-122.07213713
D3=113.28367677
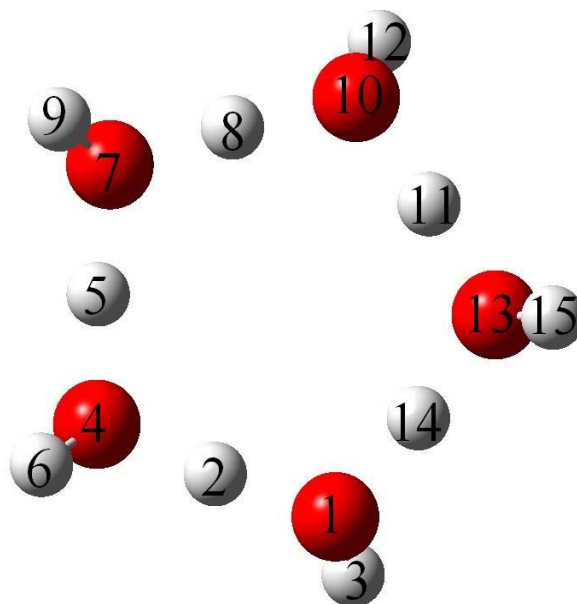
D4=-120.0253709
D5=0.48278106
D6=-124.30608452
D7=0.49250091
D8=-3.02047933
D9=119.26989316
D10=-2.88871752
D11=4.17270612
D12=-118.82169951

Table A-12: $(H_2O)_5$ reactant and transition state vibrational frequencies

S.NO	Reactant (cm^{-1})	Transition state (cm^{-1})
1	28	1609 i
2	42	38
3	70	64
4	72	116
5	179	121
6	200	344
7	208	352
8	233	371
9	235	417
10	244	482
11	272	511
12	297	581
13	301	581
14	305	585
15	427	604
16	439	683
17	468	687
18	480	689
19	537	699
20	731	745
21	795	856
22	867	921

23	890	1208
24	987	1343
25	1645	1418
26	1654	1496
27	1666	1528
28	1683	1533
29	1692	1534
30	3286	1583
31	3374	1599
32	3383	1640
33	3429	1693
34	3440	1794
35	3861	3850
36	3862	3851
37	3863	3852
38	3864	3855
39	3866	3857

Table A-13a): Reactant geometry of $(H_2O)_6$
Symbolic Z-matrix

Charge = 0 Multiplicity = 1

O								
O	1	B1						
O	2	B2	1	A1				
O	3	B3	2	A2	1	D1		
O	4	B4	3	A3	2	D2		
O	5	B5	2	A4	3	D3		
H	1	B6	6	A5	5	D4		
H	1	B7	6	A6	5	D5		
H	2	B8	1	A7	6	D6		
H	2	B9	1	A8	6	D7		
H	3	B10	2	A9	1	D8		
H	3	B11	2	A10	1	D9		
H	4	B12	3	A11	2	D10		
H	4	B13	3	A12	2	D11		
H	5	B14	4	A13	3	D12		
H	5	B15	4	A14	3	D13		
H	6	B16	1	A15	2	D14		
H	6	B17	1	A16	2	D15		

B1	2.71202279
B2	2.71166286
B3	2.71161296
B4	2.71202408
B5	2.71166735
B6	0.98603523
B7	0.96067070
B8	0.98604627
B9	0.96067431
B10	0.98604701
B11	0.96067118
B12	0.98603542
B13	0.96067071
B14	0.98604596
B15	0.96067468
B16	0.98604632
B17	0.96067038
A1	118.91785550
A2	118.93468889
A3	118.96419802
A4	59.86606844
A5	118.35569055
A6	116.97817232
A7	118.31730672
A8	116.95007655
A9	118.33058118
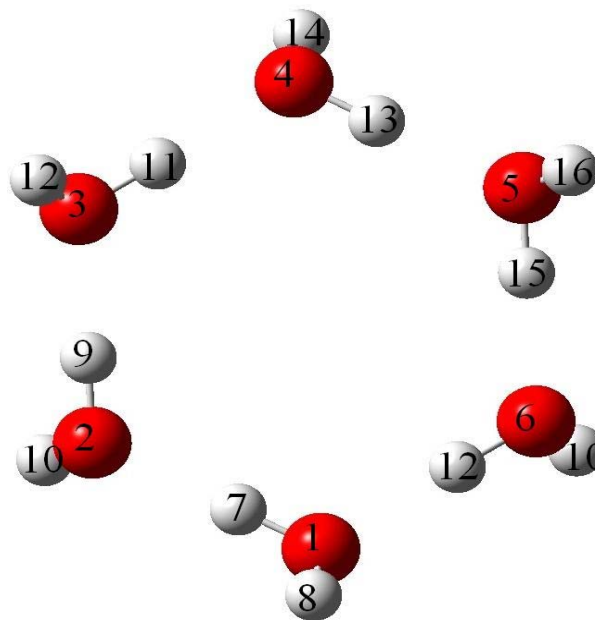
A10	117.01246117
A11	118.35608400
A12	116.97836742
A13	118.31832236
A14	116.95230318
A15	0.63542126
A16	105.47002462
D1	20.35508302
D2	-20.36167880
D3	-180.00000000
D4	20.60023125
D5	-108.20550550
D6	-20.58591018
D7	108.14793711
D8	20.57904638
D9	-108.24847489
D10	-20.59316527
D11	108.21307777
D12	20.58603656
D13	-108.15082396
D14	38.42800498
D15	-113.38478847

Table 13b): Transition state geometry of $(H_2O)_6$

Symbolic Z-matrix
 Charge = 0 Multiplicity = 1

O									
O	1	B1							
O	2	B2	1	A1					
O	3	B3	2	A2	1	D1			
O	4	B4	3	A3	2	D2			
O	5	B5	2	A4	3	D3			
H	1	B6	6	A5	5	D4			
H	1	B7	6	A6	5	D5			
H	2	B8	1	A7	6	D6			
H	2	B9	1	A8	6	D7			
H	3	B10	2	A9	1	D8			
H	3	B11	2	A10	1	D9			
H	4	B12	3	A11	2	D10			
H	4	B13	3	A12	2	D11			
H	5	B14	4	A13	3	D12			
H	5	B15	4	A14	3	D13			
H	6	B16	1	A15	2	D14			
H	6	B17	1	A16	2	D15			

B1=2.40870712
B2=2.40873992
B3=2.40857905
B4=2.40870712
B5=2.40873963
B6=1.20473967
B7=0.96057914
B8=1.20417765
B9=0.96057897
B10=1.20423253
B11=0.96057182
B12=1.2047586
B13=0.96057905
B14=1.2041895
B15=0.96057903
B16=1.20422547
B17=0.96057196
A1=119.20772743
A2=119.38340563
A3=119.60055701
A4=59.88309057
A5=119.17205013
A6=110.06400719
A7=118.8437334
A8=110.16714897
A9=118.94588501
A10=110.26861746
A11=119.17211865
A12=110.06377849
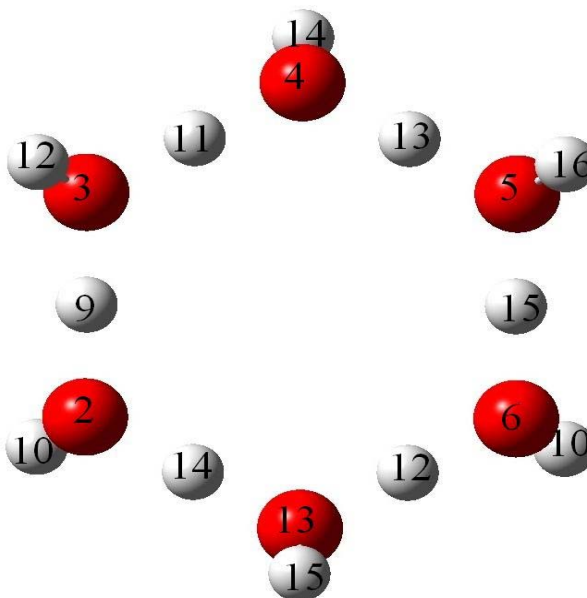
A13=118.8436247
A14=110.1666629
A15=0.44697957
A16=110.2089895
D1=15.36678157
D2=-15.42771108
D3=-179.99966286
D4=15.39867493
D5=-113.46130416
D6=-15.37352698
D7=113.3322535
D8=15.26270817
D9=-113.72461341
D10=-15.39781016
D11=113.46254297
D12=15.37335436
D13=-113.3323395
D14=3.67407032
D15=-113.68944745

Table A-14: Reactant and transition state frequencies of $(H_2O)_6$

S.NO	Reactant (cm^{-1})	Transition state (cm^{-1})
1	29	1611 i
2	30	35
3	51	38
4	51	76
5	53	83
6	90	83
7	158	142
8	187	148
9	206	161
10	212	302
11	216	326
12	217	328
13	264	442
14	269	457
15	297	459
16	301	476
17	301	535
18	333	536
19	435	635
20	454	670
21	457	671
22	474	716

………to be continued

23	481	747
24	481	749
25	793	751
26	810	754
27	817	776
28	905	1248
29	909	1252
30	982	1391
31	1639	1445
32	1650	1518
33	1651	1519
34	1678	1551
35	1679	1552
36	1695	1562
37	3271	1570
38	3352	1570
39	3352	1641
40	3412	1641
41	3412	1655
42	3432	1669
43	3863	3856
44	3863	3856
45	3863	3856
46	3864	3856
47	3864	3856
48	3865	3857

Table A15: Reactant and transition state frequencies of $(HF)_2(DF)$

S.NO	Reactant (cm^{-1})	Transition state (cm-1)
1	206	1471 i
2	209	544
3	225	547
4	404	711
5	502	767
6	530	1017
7	651	1151
8	686	1220
9	960	1391
10	2655	1517
11	3622	1740
12	3711	1930

Table A-16: Reactant and transition state frequencies of (HF)(DF)2

S.NO	Reactant (cm^{-1})	Transition state (cm^{-1})
1	205	1314 i
2	207	542
3	223	545
4	381	711
5	437	729
6	469	820
7	549	1093
8	636	1146
9	879	1228
10	2622	1254
11	2691	1561
12	3668	1787

Table A-17: Reactant and transition state frequencies of $(DF)_3$

S.NO	Reactant (cm^{-1})	Transition state (cm^{-1})
1	206	1178 i
2	206	542
3	221	542
4	383	711
5	383	729
6	473	731
7	473	928
8	530	1093
9	749	1093
10	2586	1249
11	2687	1249
12	2687	1447

Table A-18: Reactant and transition state frequencies of (HCOOD)(HCOOH)

S.NO	Reactant (cm^{-1})	Transition state (cm^{-1})
1	78	1064 i
2	173	87
3	183	229
4	212	231
5	260	300
6	278	507
7	654	571
8	714	730
9	743	795
10	995	956
11	1071	1070
12	1087	1077
13	1091	1079
14	1258	1173
15	1292	1333
16	1403	1393
17	1412	1398
18	1465	1402
19	1679	1412
20	1764	1619
21	2264	1716
22	3053	1719
23	3064	3069
24	3109	3071

Table A-19: Reactant and transition state frequencies of $(HCOOD)_2$

S.NO	Reactant (cm-1)	Transition state (cm^{-1})
1	78	915
2	171	87
3	180	227
4	211	231
5	258	300
6	275	506
7	639	569
8	683	714
9	724	782
10	766	927
11	1069	939
12	1070	972
13	1073	1077
14	1107	1092
15	1290	1129
16	1296	1220
17	1407	1392
18	1414	1398
19	1666	1408
20	1760	1424
21	2235	1673
22	2298	1711
23	3063	3068
24	3064	3071

Table A-20: Reactant and transition state frequencies of $(DCOOH)_2$

S.NO	Reactant (cm^{-1})	Transition state (cm^{-1})
1	77	1227 i
2	159	87
3	174	196
4	210	230
5	228	261
6	275	499
7	684	553
8	716	745
9	903	792
10	904	913
11	993	915
12	1016	1039
13	1020	1047
14	1028	1256
15	1263	1308
16	1268	1341
17	1428	1371
18	1471	1375
19	1669	1563
20	1746	1657
21	2269	1713
22	2273	1724
23	3041	2272
24	3153	2275

Table A-21: Reactant and transition state frequencies of $(HDO)_3$

S.NO	Reactant (cm^{-1})	Transition state (cm^{-1})
1	170	1296 i
2	179	418
3	186	419
4	204	470
5	209	535
6	239	544
7	296	651
8	311	665
9	381	720
10	427	724
11	508	855
12	650	888
13	1401	1013
14	1407	1144
15	1411	1215
16	2574	1223
17	2617	1284
18	2624	1431
19	3858	3844
20	3861	3849
21	3863	3851

Table A-22: Reactant and transition

Table A-22: Reactant and transition state frequencies of $(HDO)_4$

S.NO	Reactant (cm^{-1})	Transition state (cm^{-1})
1	52	1181 i
2	87	85
3	201	151
4	214	384
5	236	406
6	236	407
7	250	520
8	252	544
9	252	561
10	289	602
11	354	615
12	372	615
13	397	635
14	397	635
15	590	701
16	612	775
17	612	775
18	734	1060
19	1396	1118

…..to be continued

20	1405	1119
21	1405	1129
22	1419	1164
23	2430	1267
24	2499	1267
25	2499	1275
26	2526	1308
27	3858	3848
28	3858	3849
29	3858	3849
30	3858	3850

Table A-23: Reactant and transition state frequencies of (HDO)$_5$

S.NO	Reactant (cm^{-1})	Transition state (cm^{-1})
1	27	1160 *i*
2	42	38
3	68	64
4	71	114
5	173	118
6	194	333
7	202	339
8	227	350
9	229.	384
10	239	453
11	266	501
12	290	518
13	294	525
14	299	572
15	359	572
16	373	598
17	395	617
18	401	647
19	458	677
20	538	685
21	608	687

….to be continued

22	641	808
23	654	883
24	728	995
25	1396	1026
26	1405	1125
27	1408	1131
28	1423	1147
29	1426	1190
30	2396	1245
31	2459	1249
32	2465	1273
33	2497	1309
34	2505	1380
35	3858	3850
36	3859	3850
37	3861	3852
38	3861	3855
39	3863	3857

Table A-24: Reactant and transition state frequencies of (HDO) $_6$

S.NO	Reactant (cm^{-1})	Transition state (cm^{-1})
1	29	1163 i
2	30	34
3	49	37
4	50	76
5	53	81
6	89	81
7	153	115
8	181	125
9	201	141
10	207	294
11	211	317
12	212	319
13	260	433
14	264	434
15	292	435
16	295	473
17	295	528
18	323	529
19	366	560
20	384	634
21	386	643

…..to be continued

22	388	644
23	403	645
24	404	646
25	605	690
26	609	692
27	610	743
28	663	906
29	666	908
30	720	1052
31	1394	1114
32	1402	1115
33	1403	1142
34	1420	1145
35	1421	1146
36	1429	1159
37	2385	1204
38	2443	1253
39	2444	1254
40	2486	1322
41	2486	1323
42	2498	1338
43	3860	3856
44	3861	3856
45	3861	3856
46	3861	3856
47	3861	3856
48	3862	3857

Table A-25: Reactant and transition state frequencies of $(D_2O)_3$

S.NO	Reactant (cm^{-1})	Transition state (cm^{-1})
1	134	1291 i
2	149	318
3	171	329
4	174	365
5	184	498
6	206	506
7	260	527
8	268	531
9	330	562
10	421	701
11	489	852
12	629	853
13	1194	986
14	1196	1107
15	1209	1134
16	2561	1164
17	2603	1222
18	2610	1419
19	2819	2798
20	2822	2801
21	2823	2804

Table A-26: Reactant and transition state frequencies of $(D_2O)_4$

S.NO	Reactant (cm^{-1})	Transition state (cm^{-1})
1	49	1176 i
2	86	78
3	158	149
4	184	282
5	184	311
6	193	312
7	231	430
8	234	431
9	234	490
10	245	491
11	302	516
12	320	565
13	343	591
14	343	612
15	559	612
16	599	763
17	599	764

18	713	1046
19	1201	1056
20	1208	1090
21	1208	1091
22	1224	1135
23	2422	1148
24	2491	1175
25	2492	1176
26	2518	1295
27	2812	2800
28	2813	2801
29	2813	2801
30	2814	2803

Table A-27: Reactant and transition state frequencies of $(D_2O)_5$

S.NO	Reactant (cm^{-1})	Transition state (cm^{-1})
1	25	1155 i
2	39	35
3	67	58
4	70	112
5	146	117
6	150	245
7	166	255
8	175	269
9	195	313
10	221	356
11	227	424
12	236	437
13	279	494
14	282	499
15	310	501
16	321	522
17	343	539
18	350	546
19	394	651
20	529	667
21	579	667

…..to be continued

22	625	707
23	639	875
24	710	964
25	1204	1016
26	1209	1094
27	1216	1107
28	1226	1113
29	1231	1116
30	2390	1152
31	2452	1156
32	2458	1188
33	2490	1222
34	2498	1295
35	2812	2801
36	2813	2802
37	2814	2804
38	2815	2805
39	2816	2807

Table A-28: Reactant and transition state frequencies of $(D_2O)_6$

S.NO	Reactant (cm^{-1})	Transition state (cm^{-1})
1	28	-1157
2	28	31
3	48	34
4	49	69
5	49	80
6	87	80
7	134	107
8	149	117
9	150	139
10	153	214
11	188	235
12	190	237
13	213	347
14	215	348
15	224	364
16	279	428
17	280	462
18	309	467
19	314	468
20	333	510
21	335	511
22	344	515

………to be continued

23	355	597
24	356	598
25	578	688
26	585	690
27	590	727
28	650	884
29	653	886
30	705	1031
31	1201	1042
32	1207	1100
33	1207	1101
34	1223	1129
35	1224	1131
36	1233	1132
37	2379	1144
38	2437	1145
39	2437	1191
40	2479	1192
41	2479	1193
42	2492	1199
43	2813	2805
44	2813	2805
45	2814	2805
46	2814	2806
47	2814	2807
48	2815	2808

List of Publications

1. "Conformational preferences of mono-substituted cyclohydronitrogens: A theoretical study", Tapta Kanchan Roy, Susanta Ghanta, Tanmoy Mondal, **Banda Saritha**, S. Mahapatra and M. Durga Prasad, Theochem, 822, 145, (2007).

3. "On some stategies to design new high energy density molecules", T. Mondal, **B. Saritha**, S. Ghanta, T. K. Roy, S. Mahapatra and M. Durga Prasad Theochem, 897, 42 (2009).

3. "An electronic structure perspective of the promoter modes in proton transfer reactions" **B. Saritha**, M. Durga Prasad J. Phy. Chem A(To be published).

4. "π-electron reorganization during proton transfer" **B.Saritha**, M. Durga Prasad (Manuscript in preparation)

5. "Multiple proton transfers and Kinetic isotope effect" **B.Saritha**, M. Durgaprasad (Manuscript in preparation)

Posters/Oral Presentations in symposia

1 Oral presentation: 7th Annual In-house symposium organized by School of Chemistry, Chemfest 2010", Titled-"The Electronic origin of skeletal motion during hydrogen transfer in hydrogen bonded systems: Case studies of $(HF)_3$ and formic acid dimer"

2. Poster presentation: 5th Singapore India Collaborative and cooperative Chemistry Symposium" , an international symposium organized by school of chemistry, University of Hyderabad in 2009.

3. Poster presentation: "Teoretical Chemistry Symposium 2009", organized by Indian Institute of science, Bangalore, India.

4. Poster presentation: Chemfest- 4[th](2007), 5[th](2008), 6[th](2009) and 7[th](2010), Annual In-house symposium of School of Chemistry, organised by School of Chemistry, University of Hyderabad, Hyderabad, India.

5. Attended: HPC Workshop for FIST Institutes conducted during February, 2007 with CDAC at CMSD, University of Hyderabad.

6. Attended: lecture series on "Simulation in Biology and Soft Matter" November-December 2007 conducted by CMSD at University of Hyderabad.

7. Attended: HPC workshop on Tutorial "Tools for scientific Computing" on October, 2008, conducted by CMSD at university of Hyderabad.

8. Attended: "NVIDIA TESLA Super computing workshop" on July 2009 conducted by CMSD at University of Hyderabad.